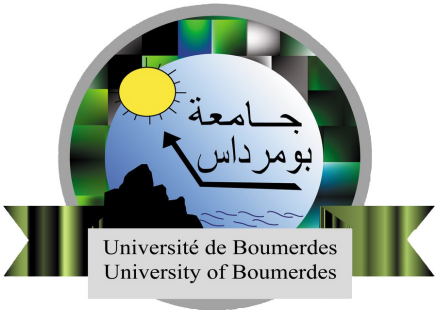

People's Democratic Republic of Algeria
Ministary of Higher Education and Scientific Research
University of M'Hamed BOUGARA - Boumerdes

Institute of Electrical Electronic Engineering IGEE ex INELEC

Final Year Project Report Presented in Partial Fulfilment of the Requirements of the Degree of

MASTER

In Power Engineering

Option : **Power Engineering**

Title:

Predictive Control with MTPA for Interior Permanent Magnet Synchronous Motor for EV Application

Presented by :

- BRAK Nour

- CHABOUR Lydia

Supervisor :

Dr AMMAR Abdelkarim

Academic year : 2023/2024

Abstract

This report investigates the application and performance of various advanced control techniques for Interior Permanent Magnet Synchronous Motors (IPMSMs) for electric vehicles application. As the requirements for energy saving and high efficiency become more popular in electric propulsion systems, the optimization of IPMSM control is essential. This study focuses on applying Maximum Torque per Ampere (MTPA) technique, with Field Oriented Control (FOC), Deadbeat Control, and Finite Control Set Model Predictive Control (FCS-MPC), on an Interior PMSM. Additionally, battery-bidirectional DC-DC converter are integrated to power the traction system. Detailed simulations were performed in this report in order to identify the effectiveness and limitations of each control method, providing a clear notion on how to optimize IPMSM control for enhanced performance in electric vehicle applications.

Dedications

This thesis is dedicated to my wonderful family, whose unwavering support and encouragement have been a constant source of strength. To my parents for their endless love, sacrifices, and belief in my dreams. To my sisters, Samira and Amel, whose constant encouragement has been invaluable. To my partner, Brak Noor, for her patience, understanding, and support throughout this journey.

Chabour Lydia

I dedicate this thesis to my precious family; my wonderful parents, my lovely siblings, and my dear friend Yasmine, who have always been a pillar in my life with their continuous love and support. I especially dedicate this work to Chabour Lydia, my hardworking and committed partner, and my loving and sweet friend.

Brak Noor

Acknowledgements

Praise to Allah the almighty for leading us in our study path and for giving us the will and patience that allowed us to complete this humble work.

We would like to express our deepest gratitude to our advisor, Ammar Abdelkarim, for his invaluable guidance, support, and encouragement throughout the course of this research. His insightful feedback and expertise were instrumental in shaping this thesis.

We also extend our appreciation to our colleagues, Teber Amine, Ticherafi Fouad, and Zidane Houssam Eddine, for their assistance, constructive critiques and suggestions, which greatly enhanced the quality of this work.

Lastly, we are profoundly grateful to our families and friends for their unwavering support and understanding during this journey. Their patience and encouragement provided us with the strength and motivation to persevere through challenging times.

Table of Contents

List of Figures

List of Tables

List of Abbreviations

AC : Alternative Current

ASSB : All Solid State Battery

BDC : Brushed DC

BEV : Battery Electric Vehicle

BLDC : Brushless DC

BMS : Battery Management System

DC : direct current

DTC : Direct Torque Control

d-q : direct-quadrature

EMF : Electromotive Force

EV : Electric Vehicle

FCEV : Fuel Cell Electric Vehicle

FCS-MPC : Finite Control Set Model Predictive Control

FOC : Field Oriented Control

HEV : Hybrid Electric Vehicle

ICE : Internal Combustion Engine

IGBTs : Insulated Gate Bipolar Transistors

IM : Induction Motor

IPMSM : interior Permanent Magnet Synchronous Motor

LC : Inductor-Capacitor

Li-ion : Lithium ion

MOSFETs : Metal Oxide Semiconductor Field Effect Transistors

MTPA : Maximum Torque per Ampere

PHEV : Plug-in Hybrid Electric Vehicle

PI : Proportional Integral

RC : Resistor-Capacitor

SoC : State of Charge

SRM : Switched Reluctance Motor

SVPWM : Space Vector Pulse Width Modulation

VSI : Voltage Source Inverter

General Introduction

Electric vehicles (EVs) have played a pivotal role in the transportation field and have become a very important industry world wide. Implementing electric vehicles is regarded as a more sustainable alternative to conventional vehicles, reducing air pollution and the dependence on nonrenewable energy sources. Electric motors are at the core of the propulsion system in EVs, and convert the electrical energy of the battery into mechanical energy to power the vehicles. Several types of electric motors with different construction and technology have been used for EVs. PMSM has attracted increasing interest and is a preferred option in comparison with other motors due to its high power, high torque, high efficiency, and simple structure [1]. To ensure the motor meets the requirements of EV systems, control systems are used, some examples include field oriented control (FOC), direct torque control (DTC) and predictive control, namely deadbeat control and finite control set model predictive control (FCS-MPC).

Field Oriented Control (FOC), also known as vector control, was proposed in the early 1970s by German engineer Felix Blaschke. FOC transforms the stator currents into a rotating reference frame using Park transform, leading to the decoupling of torque and flux. This allows for the separate control of these two parameters, which signicantly enhances the motor efficiency and dynamic performance.

Deadbeat control was proposed in the mid-20th century and is based on a discrete mathematical model of the pmsm to predict a voltage vector and apply it to the inverter through space vector pulse width modulation (SVPWM) [2]. This control

can effectively minimize overshoot, settling time, and steady-state error.

Finite Control Set Model Predictive Control (FCS-MPC) emerged in the early 2000s. FCS-MPC applies finite voltage vectors based on the characteristics of inverters to predict next instant motor stator currents by minimizing cost functions [2]. This approach allows for the explicit handling of constraints and non-linearities [3, p. 17], providing high performance.

Maximum Torque per Ampere (MTPA) is an effective strategy to optimize the performance of electric motors. The MTPA control method precisely defines the minimal stator current vector in the dq reference frame to ensure that the motor operates in the most efficient region, producing maximum torque. This leads to enhanced energy efficiency and performance, which is largely beneficial in EV applications.

This report also explores the bidirectional DC-DC converter which plays a crucial role in electric vehicle powertrain. This converter ensures efficient power transfer between the battery and the IPMSM, enabling both energy provision during acceleration and energy regeneration during braking.

Organization of the thesis:

Chapter one includes an overview of electric vehicles, electric motors and battery technology. **Chapter two** covers the modeling of different components found in an electric vehicle powertrain. **Chapter three** discusses the different control strategies for IPMSM. **Chapter four** presents the different simulations performed and discusses their results.

Chapter 1

Overview of Electric Vehicles

1.1 Introduction

Electric vehicles have existed for nearly two centuries yet it is only in the recent decades that the EV market has witnessed an increase in demand. This success is the result of the development in electric vehicle manufacturing, as well as the advancements in battery technology and electric motors.

1.2 History of EVs

The development process of the electric vehicle (EV) is interesting, as the first documented EV dates back to 1834 with inventors like Ányos Jedlik, Thomas Davenport and Robert Anderson who laid the groundwork for electric vehicles. However, they were quickly overshadowed with the surfacing of gasoline combustion engine and the mass-production techniques used by Henry Ford. These cars offered a greater range, were cheaper and had faster refueling times, which made them soar in popularity. The interest in EVs gradually deminished and ceased to receive any attention after 1920 due to several constraints; EVs had limited performance, the early batteries were heavy and had insufficient energy storage capacity, and the supporting infrastructure such as charging stations was virtually non-existent.

Modern Evs emerged in the late 20th century. The reason for this new found interest could be attributed to the growing concerns over climate change and air pollution [4]. The development of electric vehicles was made possible with the convergence of diverse technologies such as battery technology, power electronics, energy storage and vehicle to grid integration.
All of these advancements, and the efforts of companies like Tesla Motors, reshaped the automotive industry and led to the production of high-performance electric cars with an extended range and rapid charging abilities.

From humble beginnings to the forefront of innovation, the popularity of electric vehicles is only growing making its future looking brighter than ever; it could potentially become the leading type of vehicle on our roads.
Figure 1.1 shows the development of electric vehicles throughout the years.

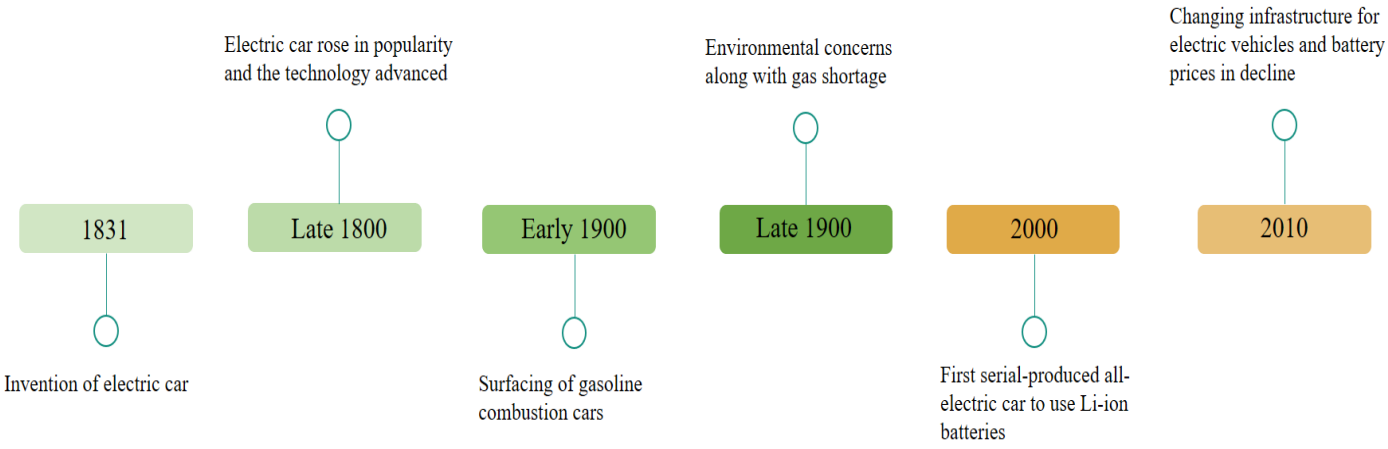

Figure 1.1: History of Electric Vehicles

1.3 Types of EVs

Electric vehicles have emerged as a transformative force in the automotive industry, revolutionizing the way we think about transportation. Central to the evolution of EVs are the diverse technologies powering their propulsion systems.

1.3.1 Battery electric vehicles (BEVs)

Battery electric vehicles also referred to as 'all-electric vehicles', run entirely on electric power and have no gasoline engine. BEVs are moved by one or more motors powered by rechargeable batteries. The battery packs are charged using electricity delivered through an EV charger. EV chargers are rated in several levels, with level-1 being the slowest and level-3 being the fastest. Most BEVs can fast charge via a level-3 charger.

The driving range of today's BEVs ranges from 50 to 400 miles per charge.

Some examples of commercialized BEVs include Tesla model 3, Nissan leaf and BMW i3. Figure 1.2 illustrates the schematics of a Battery EV.

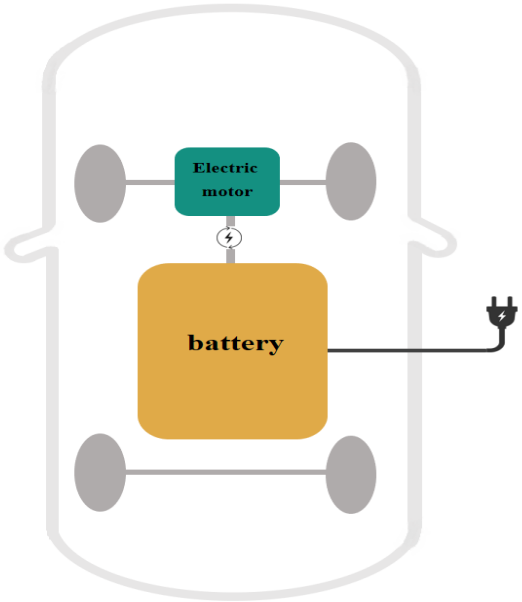

Figure 1.2: Battery electric vehicle

1.3.2 Plug-in hybrid electric vehicles (PHEVs)

Plug-in hybrid electric vehicles utilize batteries to power an electric motor and incorporate an inner combustion engine (ICE) that can recharge the batteries to enable longer driving ranges. PHEV typically runs on electricity stored in the battery until nearly depleted, then the car automatically switches over to use the ICE

and can travel several hundreds of miles on a fuel tank. All PHEV batteries can be charged by a level-1 or level-2 type of EV charger.

The electric driving range of PHEVs typically varies from 10 to 50miles.

Some examples include Chevrolet Chevy Volt and BMW i8.

Figure 1.3 illustrates the schematics of a Plug-in EV.

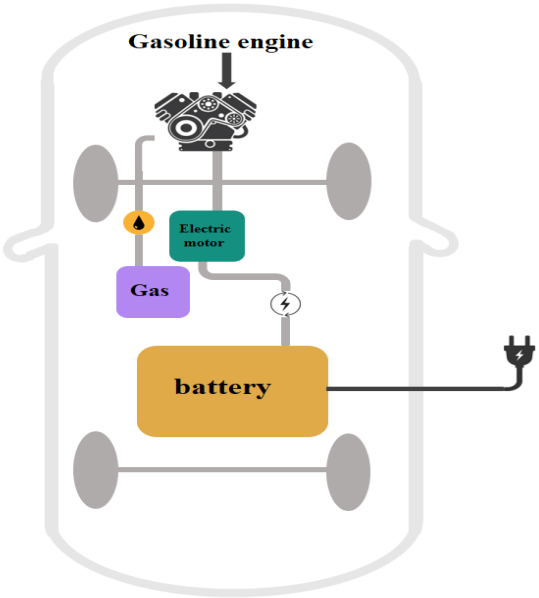

Figure 1.3: Plug-in electric vehicle

1.3.3 Hybrid Electric Vehicles (HEVs)

Hybrid electric vehicles (HEVs) use both an internal combustion engine and an electric motor which uses electricity stored in a battery pack. HEV cannot be plugged in an EV charger to charge the battery. Instead, the on-board battery pack is charged via the engine and regenerative braking. There are two types of HEVs which are mild HEV and full HEV. There are different ways that a hybrid can combine the power from an electric motor and the internal combustion engine (ICE). The most common type is Parallel Hybrid in which the mechanical power is produced from both the electric motor and the ICE. The second type is the Series Hybrid where the mechanical power is generated from the electric motor only.

HEV do not have an all electric range as they rely on their internal combustion

engine for propulsion.

Some examples of HEVs include Toyota Prius, Ford focus MHEV and Honda Insight.

Figure 1.4 illustrates the schematics of a Hybrid EV.

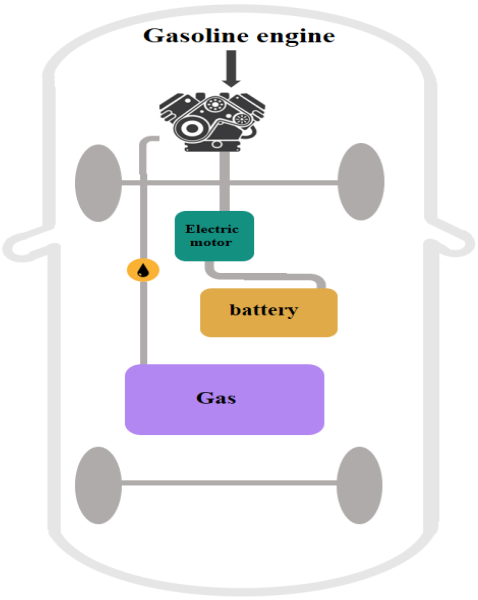

Figure 1.4: Hybrid electric vehicle

1.3.4 Fuel Cell Electric vehicles (FCEVs)

In fuel cell electric vehicles (FCEVs) the energy to propel the vehicle is stored as hydrogen and then converted into electricity by the fuel cell. Regenerative braking technology is utilized to restore the energy in the battery pack. FCEVs production is limited as of today as the refueling infrastructure is not anywhere where it needs to be to support mass production.

FCEVs typically have a range of 300miles.

Some examples include Toyota Mirai and Hyundai Nexo [5].

Figure 1.5 illustrates the schematics of a Fuel Cell EV.

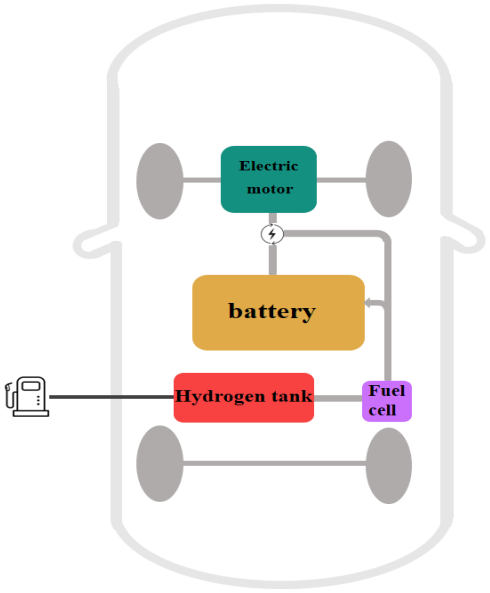

Figure 1.5: Fuel Cell electric vehicle

1.4 Battery technology

Electric vehicle (EV) batteries are the driving force behind the electrification of tranportation, representing a pivotal technology in the transition towards sustainable mobility. These advanced energy storage systems play a crucial role in powering electric vehicles, offering a cleaner and more efficient alternative to traditional internal combustion engines. As the demand for EVs continues to rise, understanding the fundamentals of electric vehicle batteries is essential to grasp their significance in shaping the future of transportation.

1.4.1 Electric vehicle battery types

Electric vehicle batteries are the backbone of the electric mobility, providing the energy needed to power these vehicles. They come in various types, each with its own advantages and considerations.

1.4.1.1 Lithium-ion batteries

One prevalent type of EV battery is lithium-ion (Li-ion) battery, known for its high energy density, relatively lightweight, and long cycle life. Li-on batteries have a high energy per weight ratio, a parameter which is very important for electric car batteries. This translates to longer driving ranges and improved performance compared to other battery technologies. Additionally, lithium-ion batteries offer fast charging capabilities and a low self-discharging level which allows to hold a full charge. Despite their many benefits, lithium-ion batteries also face challenges such as overheating from overcharging the batteries or exposure to extreme temperatures, causing thermal runaway, which can lead to fires or explosions [6].

Working principle of Lithium-ion batteries A lithium-ion battery is essentially a concentration battery. The working principle is shown in the figure below. Lithium ions are detached from the positive plate when the battery charges and inserted into the negative electrode through the electrolyte solution. At that moment, the negative electrode is in a lithium-rich state and the electrons will move to the negative pole of the battery through the external circuit, and charge compensation will be performed on the negative pole, thereby maintaining the electrical balance of the negative pole. When the battery is discharged, lithium ions fall off the negative electrode plate and are inserted into the positive electrode after passing through the electrolyte solution. At this time, the positive electrode is in a lithium-rich state [7, p. 12].

The figure 1.6 explains the working principle of a Lithium-ion cell.

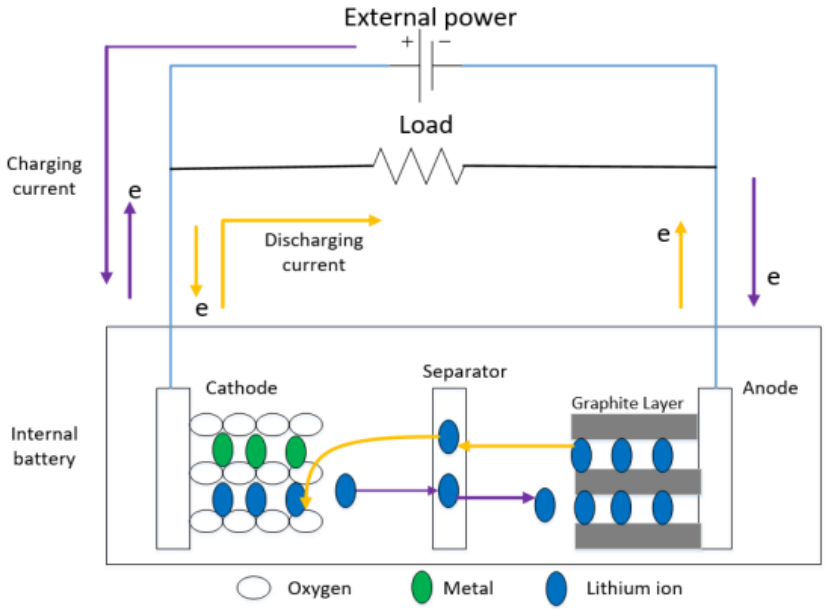

Figure 1.6: Lithium-ion cell working principle

1.4.1.2 All solid state batteries

All solid state batteries have emerged as a promising solution to address the limitations of traditional lithium-ion batteries. By replacing the liquid electrolyte found in li-ion batteries with solid materials like ceramics and solid polymers, ASSBs aim to enhance safety, increase and extend the overall lifespan of energy storage systems. While the potential advantages of ASSBs for electric vehicles are promising, several challenges remain to be addressed before widespread commercialization. These include optimizing manufacturing processes, improving material performance and stability, and reducing production costs to make solid-state batteries economically viable for mass-market EVs [6].

Figure 1.7 shows the different components of the lithium-ion battery and the all-solid-state battery.

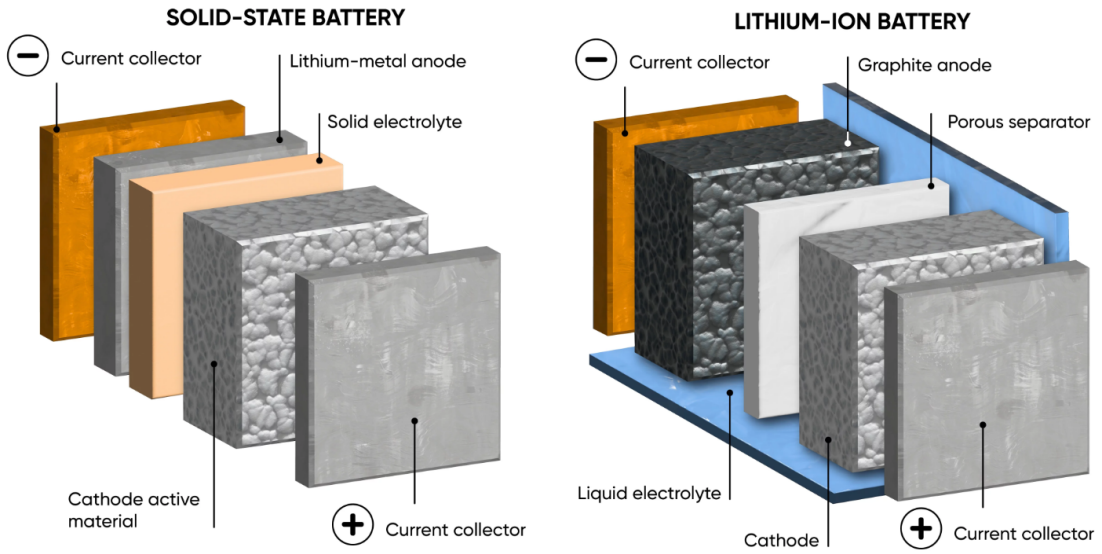

Figure 1.7: A schematic comparison between the structure of a traditional lithium-ion battery and an all-solid-state battery

1.4.2 Battery management system

Battery management system (BMS) is a technology system that maximizes the life of electric vehicle battery and its characteristics. It is strongly recommended that all battery powered electric vehicles install BMS. The aim is to ensure the battery stays within the ideal working parameters. Some special functions of the battery management system include:

- Charge balancing, to ensure all cells complete charging at the same time then to prevent damage through overcharging.
- Active balancing, in which energy is transferred from stronger cells to weaker cells, to ensure all cells reach the maximum discharge point at the same time.
- Temperature monitoring (temperature monitoring), to avoid damage due to overheating.
- Low-voltage cut-off, a way to isolate a battery when any cell reaches the recommended minimum voltage, and to avoid damage due to overuse.
- State of charge (SoC) monitoring of all battery cells for electric cars. Through

monitoring voltage and current, the remaining capacity of each cell can be calculated [6].

1.5 Overview of electric vehicle motors

Electric drives are the core of electric vehicles. They convert the electrical energy from the vehicle's batteries into a mechanical energy. One of the critical components of electric drives is the motor. EV traction motors are required to have high efficiency, high power density, low manufacturing cost and downsized volume.

1.5.1 Types of Electric vehicle motors

Various types of motors have been used in EVs, each offering their own characteristics and specifications.

1.5.1.1 Brushed DC motors

They are composed of the stator that contains permanent magnets, the rotor made out of coiled wires, the commutator which makes a connection between the rotor and the brushes that are connected to the DC power source in order to switch the direction of the flow of the current in the armature windings.
BDC motors offer simplicity, affordability, good starting torque and are well suited for applications requiring straightforward speed and torque regulation. These motors however suffer from low efficiency and limited lifespan due to brush wear

1.5.1.2 Brushless DC motors

They consist of a stator that contains the coiled wires, the rotor that has a permanent magnet mounted on its surface, a motor controller and position sensors. As the stator is energized with direct current, the rotor will rotate and the motor controller will monitor the rotation of the rotor such that it will selectively energize the

coil in a sequence that results in the rotation of the magnetic field. The interaction between the rotating magnet field and the permanent magnet, generates torque that causes the rotor to continue on rotating.

BLDC motors provide high efficiency, a long lifespan, low maintenance and improved reliability.

1.5.1.3 Permanent Magnet Synchronous motors

They contain a stator that has windings connected to the power source and a rotor that has permanent magnets placed within its structure. When alternating current is applied to the stator windings, it creates a rotating magnetic field. This rotating magnetic field will interact with the permanent magnets of the rotor, creating torque that causes the rotation of the rotor.

PMSMs can be seperated into two main categories based on the placement of the magnets in the rotor as illustated in figure 1.8.

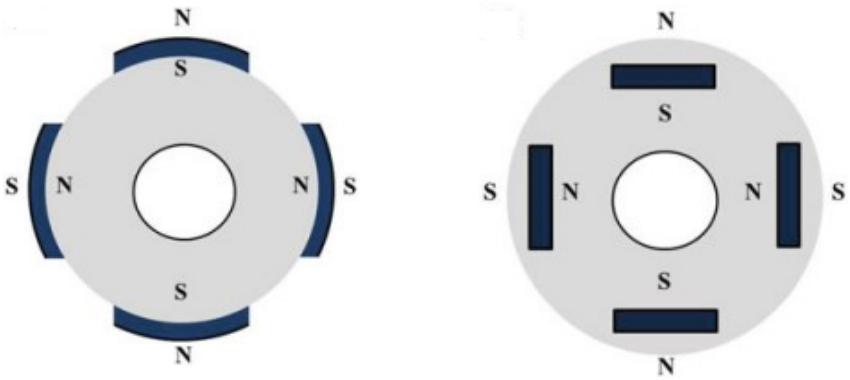

(a) Surface-mounted PMSM (b) Interior PMSM

Figure 1.8: Types of PMSM

- Surface permanent magnet motors have the magnet affixed to the exterior of the rotor surface, resulting in weak mechanical strength which limits the maximum mechanical speed. In addition, these motors exhibit poor magnetic saliency (Ld=Lq), making the motor designs rely almost completely on the magnetic torque component to produce torque.

- Interior permanent magnet motors have the permanent magnet embedded into the rotor itself, making the IPMSM very mechanically sound and suitable for operating at very high speeds. These motors also are defined by their relatively high magnetic saliency ratio (Lq>Ld), which gives the IPMSM the ability to generate torque by taking advantage of both the magnetic and reluctance torque components [8].

1.5.1.4 Induction motors

They include a stator that has copper windings and a rotor made of conductive materials. When an alternating current is applied on the windings, it will create a rotating magnetic field. This field will induce current in the rotor which also creates its own magnetic field. The interaction between the two fields will create the torque, leading to the rotation of the motor.
IMs provide high starting torque and can operate efficiently over a wide range of speeds, without the need for complex control systems. The downsides of induction motors are lower efficiency at low speeds and relative inaccuracy of the speed control.

1.5.1.5 Switched Reluctance motors

They are made up of a stator with multiple sets of windings and a rotor with salient poles or teeth. When current is applied to the windings, it creates a magnetic field, which will make the rotor experience a reluctance in aligning itself with the magnetic field. The position of the rotor is monitored and the stator windings are energized sequentially using power electronics. This rotation will cause the rotor to continuously try to align itself with the magnetic field. This movement will create a torque that drives the rotor to rotate. SRMs have a relatively simple construction and are highly robust. However, they require sophisticated control algorithms and may produce audible noise particularly at higher speeds.
Here's a comparison between these motors based on different characteristics:

Table 1.1: Comparison of EV Motors

Types of motors	BDC	BLDC	PMSM	IM	SRM
Efficiency	Low	High	High	Low at low speeds.High at high speeds	Depends on system design
Reliability	Low	High	High	High	High
Maintenance	High	Low	Low	Low	Low
Cost	Low	Moderate	High	Low	Variable
Torque	Moderate	Smooth	Smooth	Smooth at high speeds.Less responsive at low speeds	Good
Speed range	Limited	Wide	Wide	Wide	Wide

1.6 Conclusion

In this chapter, we explored the development of electric vehicles from their emergence to the different types seen in the modern world, the various motors used to drive them with a description of their characteristics, and the battery technology utilized for EVs.

Chapter 2

Modeling of Electric Vehicle Powertrain

2.1 Introduction

Powertrain refers to the set of components that generate the power and deliver it to the road surface. Among the key elements of a powertrain are the electric motor; interior pmsm is a favored option for its high efficiency and reliability, and the dc-ac inverter that transmits the electrical energy from the battery to the motor.

2.2 Vehicle Dynamics

A moving vehicle is subject to various forces that influence its motion and stability. The forces acting on the vehicle are shown in figure 2.1.

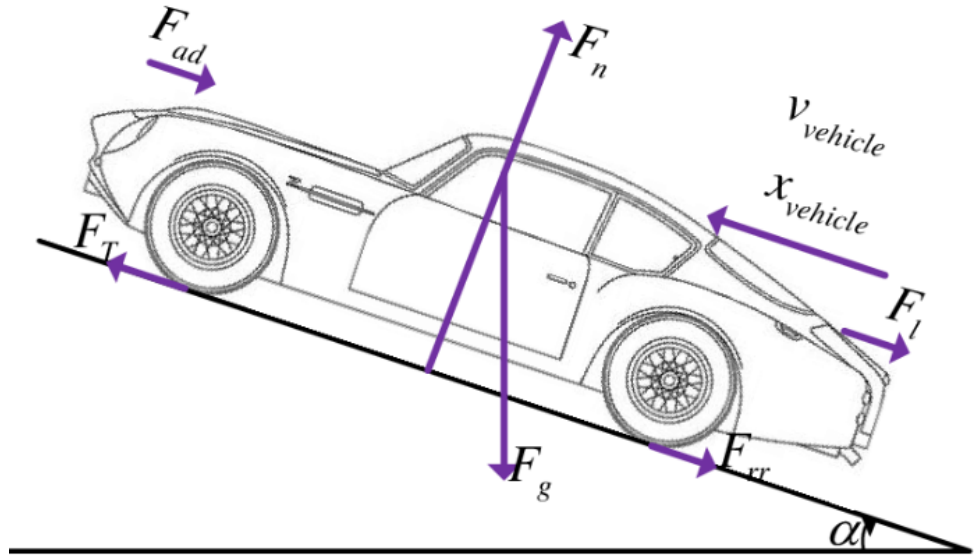

Figure 2.1: The forces acting on a moving vehicle

- F_{ad} is the aerodynamic drag force which is the resistive force that opposes the vehicle's motion through the air. It depends on the front area of the vehicle, side mirrors, ducts, and many other factors. This force can be calculated using the equation:

$$F_{ad} = 12\rho A C_d (V + V_w)^2 \tag{2.1}$$

  Where ρ is the density of the air (kg/m^3), A is the front area of the vehicle (m^2), C_d is the drag coefficient constant, V is the vehicle longitudinal speed (m/s), and V_w is the wind speed (m/s).

- F_N is the lift force which is perpendicular to the direction of motion. It can increase the upward force, which can reduce traction and stability.

- F_l the inertia force is the resistive force that opposes the direction of the vehicle's acceleration. It can be expressed using Newton's Second Law of motion:

$$F_l = m \cdot a \tag{2.2}$$

  Where m is the mass of the vehicle (kg), and a is the acceleration of the object (m/s^2).

- F_{rr} is the rolling resistance force that is due to the friction between the vehicle's tires and the ground surface. It can be influenced by the deformation of the wheel or tire and the surface it rolls on, as well as the tire composition and the vehicle's weight. It can be expressed by:

$$F_{rr} = mgf_r cos(\alpha) \tag{2.3}$$

  Where g is the gravitational acceleration (m/s^2), f_r is the rolling resistance coefficient.

- F_g is the gravitational force that attracts the vehicle to the center of the earth. It is given by:

$$F_g = mgsin(\alpha) \tag{2.4}$$

- F_t is the traction force that is generated by the tires as they interact with the road surface, propelling the vehicle forward or backward. This force is critical for accelerating, decelerating, and maintaining control of the vehicle.
  The force required for the movement of the vehicle must exceed the resistive forces present in the system. This traction force can be formulated as follows:[9]

$$F_t = F_l + F_g + F_{rr} + F_{ad} \tag{2.5}$$

2.3 Modeling of IPMSM

2.3.1 IPMSM mathematical model in the stationary reference frame

Modeling of IPMSM is a critical aspect of designing and analyzing these high performance motors. The primary focus of IPMSM modeling includes: electrical modeling, electromagnetic modeling, and mechanical modeling. The conventional

dynamic and mathematical machine models are presented by introducing the following assumptions:

- The distribution of the magneto-motive force in the air gap is sinusoidal.
- Slot harmonics effects are neglected.
- Temperature effects on the machine are neglected.
- Hysteresis and eddy currents in the iron core are neglected.
- Magnetic behavior of the machine is linear.
- Rotor speed of the machine is constant.

The general voltage equations of a balanced three-phase IPMSM are:

$$\begin{aligned} v_a &= Ri_a(t) + \frac{d\lambda_a(t,\theta_e)}{dt} \\ v_b &= Ri_b(t) + \frac{d\lambda_b(t,\theta_e)}{dt} \\ v_c &= Ri_c(t) + \frac{d\lambda_c(t,\theta_e)}{dt} \end{aligned} \tag{2.6}$$

Where:

- θ_e is the rotor electrical position (given by the product of the number of pole pairs p and the the mechanical position θ_r).
- v_a, v_b, v_c are the instantaneous phase voltages.
- i_a, i_b, i_c are the instantaneous phase currents.
- $\lambda_a, \lambda_b, \lambda_c$ are the instantaneous magnetic phase flux linkage.
- R is the phase resistance, that is equal for all three phases.

Flux linkage to the stator phases are both a function of the currents circulating in each stator phase and of the magnetic flux emanating from the rotor permanent magnets. It is assumed that the rotor and the stator of the machine exhibit constant

magnetic permeability.

The flux linkage can be expressed with the following relationships:

$$\begin{aligned} \lambda_a &= \lambda_{a,i}(t) + \lambda_{PMa}(t) \\ \lambda_b &= \lambda_{b,i}(t) + \lambda_{PMb}(t) \\ \lambda_c &= \lambda_{c,i}(t) + \lambda_{PMc}(t) \end{aligned} \tag{2.7}$$

Where λ_{PMn} is the flux linkage produced by the permanent magnets expressed as:

$$\begin{aligned} \lambda_{PMa} &= \lambda_{PM}\cos(p\theta_r) \\ \lambda_{PMb} &= \lambda_{PM}\cos(p\theta_r - \frac{2}{3}\pi) \\ \lambda_{PMc} &= \lambda_{PM}\cos(p\theta_r - \frac{4}{3}\pi) \end{aligned} \tag{2.8}$$

Where λ_{PM} represents the peak value of flux linkage of each phase due to the permanent magnets.

The flux linkage produced by stator current excitation $\lambda_{n,i}$ are expressed as:

$$\begin{aligned} \lambda_{a,i} &= L_{aa}i_a + L_{ab}i_b + L_{ac}i_c \\ \lambda_{b,i} &= L_{ba}i_a + L_{bb}i_b + L_{bc}i_c \\ \lambda_{c,i} &= L_{ca}i_a + L_{cb}i_b + L_{cc}i_c \end{aligned} \tag{2.9}$$

Where L_{aa}, L_{bb}, L_{cc} are the self inductances of the three phases, L_{ab}, L_{bc} and L_{ac} are the mutual inductances between one phase to the other ones.

The relationships described above can also be expressed in matrix form as follows:

$$\begin{bmatrix} v_a \\ v_b \\ v_c \end{bmatrix} = \begin{bmatrix} R & 0 & 0 \\ 0 & R & 0 \\ 0 & 0 & R \end{bmatrix} \begin{bmatrix} i_a \\ i_b \\ i_c \end{bmatrix} + \frac{d}{dt} \begin{bmatrix} \lambda_a \\ \lambda_b \\ \lambda_c \end{bmatrix} \tag{2.10}$$

$$\begin{bmatrix} \lambda_a \\ \lambda_a \\ \lambda_a \end{bmatrix} = \begin{bmatrix} L_{aa} & L_{ab} & L_{ac} \\ L_{ba} & L_{bb} & L_{bc} \\ L_{ca} & L_{cb} & L_{cc} \end{bmatrix} \begin{bmatrix} i_a \\ i_b \\ i_c \end{bmatrix} + \begin{bmatrix} \lambda_{PMa} \\ \lambda_{PMb} \\ \lambda_{PMc} \end{bmatrix} \tag{2.11}$$

The expressions 2.10 and 2.11 can be written in compact form:

$$[v] = [R][i] + \frac{d[\psi]}{dt} \tag{2.12}$$

$$[\psi] = [L][i] + [\lambda] \tag{2.13}$$

Replacing 2.12 and 2.13, we obtain the following expression:

$$\begin{aligned} [v] = [R][i] + \frac{d}{dt}([L][i] + [\lambda]) = [R][i] + \frac{d[L]}{dt}[i] + \frac{d[i]}{dt}[L] + \frac{d[\lambda]}{dt} = \\ [R][i] + \frac{d\theta_r}{dt}\frac{d[L]}{d\theta_r}[i] + \frac{d[i]}{dt}[L] + \frac{d\theta_r}{dt}\frac{d[\lambda]}{d\theta_r} = \\ [R][i] + \omega_r \frac{d[L]}{d\theta_r}[i] + [L]\frac{d[i]}{dt} + \omega_r \frac{\lambda}{d\theta_r} \end{aligned} \tag{2.14}$$

Where:

- [R][i] are the drop voltages in each phase;
- [L]$\frac{d[i]}{dt}$ are the back electromotive forces self and mutually induced in the stator windings;
- $\omega_r \frac{d[L]}{d\theta_r}$[i] are the rotational back electromotive forces due to the anisotropy [1] of the machine;
- $\omega_r \frac{d[\lambda]}{d\theta_r}$ are the rotational back electromotive forces induced by the flux of the permanent magnets

The expression of the input power of IPMSM can be obtained as follows:

$$[P_e] = [i]^T[v] = [i]^T[R][i] + [i]^T[L]\frac{d[i]}{dt} + \omega_r[i]^T\frac{d[L]}{d\theta_r}[i] + \omega_r[i]^T\frac{d[\lambda]}{d\theta_r} \tag{2.15}$$

[1] The salient-pole structure of ipmsm leads to different magnetic reluctance along axes in different directions affecting the distribution of magnetic flux and thus the back emf.

Where:

- $P_{cu} = [i]^T[R][i]$ represents the joule losses in the stator windings;
- $[i]^T[L]\frac{d[i]}{dt}$ represents the power stored in the magnetic field;
- $P_m = \omega_r[i]^T\frac{d[L]}{d\theta_r}[i] + \omega_r[i]^T\frac{d[\lambda]}{d\theta_r}$ represents the mechanical power of the shaft.

2.3.2 IPMSM mathematical model in dqo synchronous reference frame:

Due to the salient nature of the rotor, the inductances are a function of the position of the rotor. Thus, the mathematical model of the IPMSM is time-varying and non-linear which makes the analysis of the machine challenging. This difficulty is overcome by transforming the equations describing the machine into a reference frame, where the inductances are not a function of time. For synchronous machine, this reference frame is that of the rotor; the stator voltages, currents, and inductances will be projected onto the rotor side of the machine.

This transformation is known as the Park transformation which allows the transition from a three-phase stator reference system to a two-phase reference frame system that is rotating at the electrical rotor speed ω_e and with the real axis coincident to the polar rotor axis. To obtain the Park model, a first coordinate transformation is carried out from the stator reference system (a,b,c) to the fixed two-phase reference system (α, β). With such transformation, there are only two windings arranged at 90 degrees. However, the inductive coefficients are still a function of the angular position of the rotor. Therefore, a further transformation is needed which allows to express stator and rotor quantities under a single reference. A system of axes (dqo) rotating integrally with the rotor is considered.

These transformations are shown in the figure 2.2:

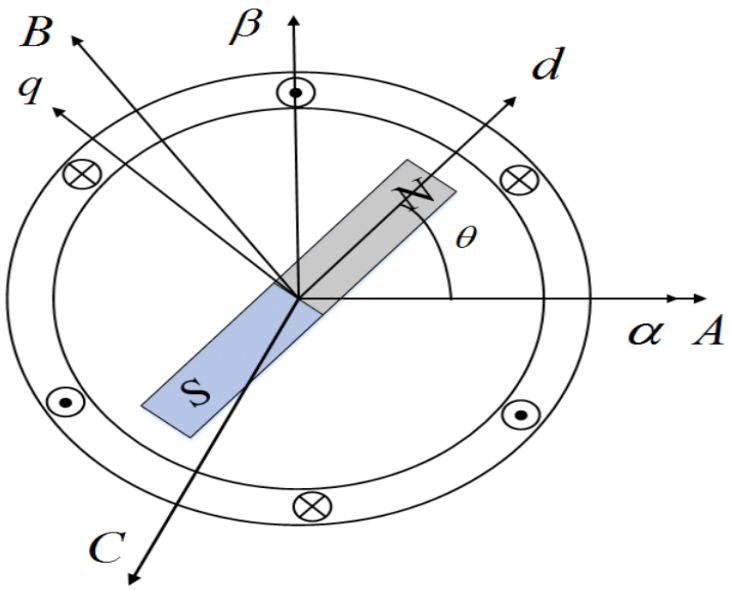

Figure 2.2: Transformation of coordinates from abc to $\alpha\beta$ to dqo

The transformation of the quantities from the three-phase reference system (a,b,c) to the reference system (d,q,o) is carried out through the following transformation matrix:

$$[T] = \frac{2}{3}\begin{bmatrix} cos(p\theta_r) & cos(p\theta_r - \frac{2}{3}\pi) & cos(p\theta_r - \frac{4}{3}\pi) \\ -sin(p\theta_r) & -sin(p\theta_r - \frac{2}{3}\pi) & -sin(p\theta_r - \frac{4}{3}\pi) \\ \frac{1}{2} & \frac{1}{2} & \frac{1}{2} \end{bmatrix} \tag{2.16}$$

It is also possible to define the inverse matrix which allows the transformation of the quantities from the coordinate system (d,q,o) to the three-phase coordinate system (a,b,c):

$$[T]^{-1} = \frac{2}{3}\begin{bmatrix} cos(p\theta_r) & -sin(p\theta_r) & 1 \\ cos(p\theta_r - \frac{2}{3}\pi) & -sin(p\theta_r - \frac{2}{3}\pi) & 1 \\ cos(p\theta_r - \frac{4}{3}\pi) & -sin(p\theta_r - \frac{4}{3}\pi) & 1 \end{bmatrix} \tag{2.17}$$

Applying the aforementioned transformation of coordinates to the IPMSM mathe-

matical model, the flux equation is:

$$[\lambda_{d,q,o}] = [T][\lambda_{a,b,c}] = [T][L][i_{a,b,c}] + [T][\lambda_{a,b,c}] = [T][L][T]^{-1}[i_{d,q,o}] = \\ = \begin{bmatrix} L_d & 0 & 0 \\ 0 & L_q & 0 \\ 0 & 0 & L_o \end{bmatrix} \begin{bmatrix} i_d \\ i_q \\ i_o \end{bmatrix} + \begin{bmatrix} \lambda_{PM} \\ 0 \\ 0 \end{bmatrix} \tag{2.18}$$

Where each inductance component is:

$$L_d = L_s + M_s + \frac{3}{2}L_m \tag{2.19}$$

$$L_q = L_s + M_s - \frac{3}{2}L_m \tag{2.20}$$

$$L_o = L_s - 2M_s \tag{2.21}$$

$$L_s = L_{\sigma s} + L_{mso} + \frac{3}{2}L_m \tag{2.22}$$

where $L_{\sigma s}$ is the leakage inductance and L_{ms0} and L_m represent the constant component and the amplitude of the anisotropy of the magnetization inductance respectively.

The voltage balance equations results:

$$[v_{d,q,o}] = [T][v_{a,b,c}] = [T][R][i_{a,b,c}] + [T]\frac{d[\lambda_{a,b,c}]}{dt} = \\ = [T][R][T]^{-1}[i_{d,q,o}] + [T]\frac{d[T]^{-1}[\lambda_{d,q,o}]}{dt} = \\ = \begin{bmatrix} R & 0 & 0 \\ 0 & R & 0 \\ 0 & 0 & R \end{bmatrix} \begin{bmatrix} i_d \\ i_q \\ i_o \end{bmatrix} + \frac{d}{dt} \begin{bmatrix} \lambda_d \\ \lambda_q \\ \lambda_o \end{bmatrix} + [T]\omega_r \frac{d[T]^{-1}}{d\theta} \begin{bmatrix} \lambda_d \\ \lambda_q \\ \lambda_o \end{bmatrix} =$$

$$= \begin{bmatrix} R & 0 & 0 \\ 0 & R & 0 \\ 0 & 0 & R \end{bmatrix} \begin{bmatrix} i_d \\ i_q \\ i_o \end{bmatrix} + \frac{d}{dt} \begin{bmatrix} \lambda_d \\ \lambda_q \\ \lambda_o \end{bmatrix} + p\omega_r \begin{bmatrix} -\lambda_q \\ \lambda_d \\ 0 \end{bmatrix} \tag{2.23}$$

Replacing 2.18 in 2.23, the voltage equation became:

$$\begin{bmatrix} v_d \\ v_q \\ v_o \end{bmatrix} = \begin{bmatrix} R & 0 & 0 \\ 0 & R & 0 \\ 0 & 0 & R \end{bmatrix} \begin{bmatrix} i_d \\ i_q \\ i_o \end{bmatrix} + \begin{bmatrix} L_d & 0 & 0 \\ 0 & L_q & 0 \\ 0 & 0 & L_o \end{bmatrix} \frac{d}{dt} \begin{bmatrix} i_d \\ i_q \\ i_o \end{bmatrix} + p\omega_r \begin{bmatrix} -L_q i_q \\ L_d i_d + \lambda_{PM} \\ 0 \end{bmatrix} \tag{2.24}$$

The balance of powers in the (d,q,o) coordinate system is given by the following expression:

$$P_i = [i_{a,b,c}]^T [v_{a,b,c}] = [i_{d,q,o}]([T]^{-1})^T [T]^{-1} [v_{d,q,o}] = \frac{3}{2}(v_d i_d + v_q i_q + v_o i_o) \tag{2.25}$$

Developing this equation it is possible to obtain:

$$P_i = [i_{a,b,c}]^T [v_{a,b,c}] = [i_{d,q,o}]([T]^{-1})^T [T]^{-1} [v_{d,q,o}] =$$

$$= [i_{d,q,o}]([T]^{-1})^T [T]^{-1} \left\{ [R][i_{d,q,o}] + [L_{d,q,o}] \frac{d}{dt} [i_{d,q,o}] + p\omega_r \begin{bmatrix} -\lambda_q \\ \lambda_d \\ 0 \end{bmatrix} \right\} =$$

$$= [i_{d,q,o}]([T]^{-1})^T [T]^{-1} [R][i_{d,q,o}] + [i_{d,q,o}]([T]^{-1})^T [T]^{-1} [L_{d,q,o}] \frac{d}{dt} [i_{d,q,o}] \tag{2.26}$$

$$+ [i_{d,q,o}]([T]^{-1})^T [T]^{-1} p\omega_r \begin{bmatrix} -\lambda_q \\ \lambda_d \\ 0 \end{bmatrix}$$

Where the first term represents the joule losses in the stator windings P_{cu}, the second term represents variation in the time unit of the energy stored in the magnetic field produced by the armature ampere-turns (P_{ms}) and the last term represents the

output mechanical power P_m.

The power P_m is equal to:

$$P_m = [i_d, q, o]([T]^{-1})^T[T]^{-1}p\omega_r \begin{bmatrix} -\lambda_q \\ \lambda_d \\ 0 \end{bmatrix} = \frac{3}{2}p\omega_r[\lambda_d i_q - \lambda_q i_d] = \frac{3}{2}p\omega_r[\lambda_{PM} i_q + (L_d - L_q) i_d i_q] \tag{2.27}$$

From this equation, it is possible to obtain the expression of electromagnetic torque:

$$T_{em} = \frac{3}{2}p[\lambda_d i_q - \lambda_q i_d] = \frac{3}{2}[\lambda_{PM} i_q + (L_d - L_q) i_d i_q] \tag{2.28}$$

The expression of electromagnetic torque is composed of two components, where the first, named magnetic torque, is a function of the flux linkage produced by permanent magnets and of q-axis current and the second term, named reluctance torque, is a function of both dq-axis currents and the saliency of the machine.

Below, all the equations of the IPMSM conventional dynamic and mathematical model, including the mechanical balance equation, are reported:

$$v_d = Ri_d + L_d\frac{di_d}{dt} - p\omega_r L_q i_q \tag{2.29}$$

$$v_q = Ri_q + L_q\frac{di_q}{dt} + p\omega_r L_d i_d + p\omega_r \lambda_{PM} \tag{2.30}$$

$$T_{em} = \frac{3}{2}p[\lambda_{PM} i_q + (L_d - L_q) i_d i_q] \tag{2.31}$$

$$T_{em} = T_L + B\omega_r + J\frac{d\omega_r}{dt} \tag{2.32}$$

$$\frac{d}{dt}\theta_r = \omega_r \tag{2.33}$$

Where T_L is the load torque, B is the viscous friction coefficient and J is the equivalent rotor inetia constant.

The equivalent dq-axis circuits of the mathematical model of the IPMSM are presented in figure 2.3 [10, p. 11–19]

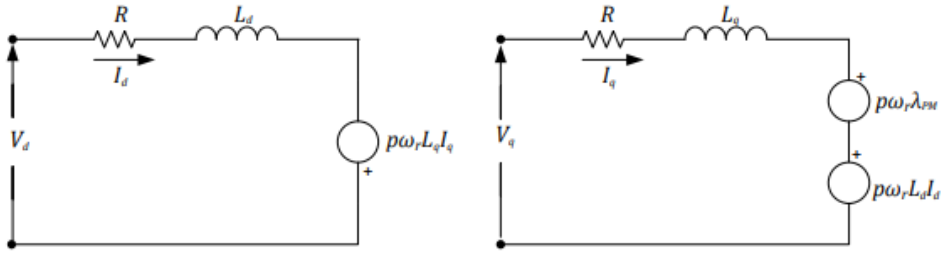

Figure 2.3: Equivalent circuit of ipmsm using the mathematical model

2.4 Voltage Source Inverter

Inverters are essential components in electric vehicle (EV) powertrains and various other applications, serving as the connection between the DC power source and the electric motor. An inverter converts direct current (DC) from the source into alternating current (AC) with precise control over frequency and voltage, letting the motor achieve optimal performance across a wide range of speeds and loads.

Inverter used for AC motor drive applications typically require a 3-phase 2-level voltage source inverter which converts DC power into 3-phase AC power with 2 voltage levels (typically V_{dc} and $-V_{dc}$) [11]

The basic structure of an inverter can be seen in figure 2.4.

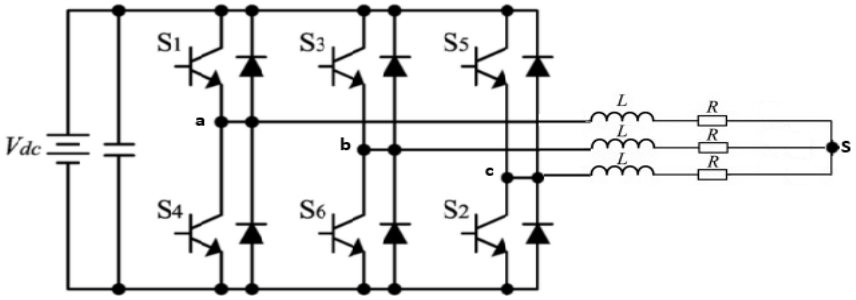

Figure 2.4: Three-phase inverter circuit

To generate a three-phase AC supply, the inverter operates with a 120-degree phase shift between its three arms. This means that each switch in the circuit is turned on and off in a synchronized manner, creating a balanced AC output [12].

2.5 Space Vector Pulse Width Modulation

Space vector pulse width modulation (SVPWM) is an advanced technique used to control the switching of inverters. SVPWM generates a more efficient and higher quality AC waveform compared to traditional PWM. This technique involves calculating the position of the reference voltage vector in the space vector diagram and determining the switching states of the inverter's semiconductor devices to produce the desired output voltage. SVPWM maximizes the use of the DC bus voltage, resulting in a higher output voltage and better utilization of the inverter's capacity. Additionally, it reduces harmonic distortion and switching losses, leading to improved performance and efficiency of EV drives.

The two-level VSI consists of 6 switching devices including 3 upper and 3 lower devices respectively. Only one of the two power switches turns on in each phase. Therefore, there is a total of 2^3 (8) combinations of on/off states which corresponds to the different space vectors. The latter are elaborated in Table 2.1 by using the following relationships: [13]

$$\begin{cases} v_{ab} = v_a - v_b \\ v_{bc} = v_b - v_c \\ v_{ca} = v_c - v_a \end{cases} \tag{2.34}$$

$$\begin{cases} v_{as} = \frac{(v_{ab}-v_{ca})}{3} \\ v_{bs} = \frac{(v_{bc}-v_{ab})}{3} \\ v_{cs} = \frac{(v_{ca}-v_{bc})}{3} \end{cases} \tag{2.35}$$

$$v_r(t) = \frac{2}{3}(v_a(t) + v_b(t)e^{\frac{2\pi}{3}} + v_c(t)e^{\frac{4\pi}{3}}) \tag{2.36}$$

Table 2.1: Inverter Switching States and Machine Voltages

States	S_a	S_b	S_c	V_a	V_b	V_c	V_{ab}	V_{bc}	V_{ca}	V_{as}	V_{bs}	V_{cs}	V_r
I	1	0	0	V_{dc}	0	0	V_{dc}	0	-V_{dc}	$\frac{2}{3}V_{dc}$	-$\frac{1}{3}V_{dc}$	-$\frac{1}{3}V_{dc}$	$\frac{2}{3}V_{dc}e^{j0}$
II	1	0	1	V_{dc}	0	V_{dc}	V_{dc}	-V_{dc}	0	$\frac{2}{3}V_{dc}$	-$\frac{1}{3}V_{dc}$	-$\frac{1}{3}V_{dc}$	$\frac{2}{3}V_{dc}e^{j\frac{\pi}{3}}$
III	0	0	1	0	0	V_{dc}	0	-V_{dc}	V_{dc}	-$\frac{1}{3}V_{dc}$	-$\frac{1}{3}V_{dc}$	$\frac{2}{3}V_{dc}$	$\frac{2}{3}V_{dc}e^{j\frac{2\pi}{3}}$
IV	0	1	1	0	V_{dc}	V_{dc}	-V_{dc}	0	V_{dc}	-$\frac{2}{3}V_{dc}$	$\frac{1}{3}V_{dc}$	$\frac{1}{3}V_{dc}$	$\frac{2}{3}V_{dc}e^{j\pi}$
V	0	1	0	0	V_{dc}	0	-V_{dc}	V_{dc}	0	-$\frac{1}{3}V_{dc}$	$\frac{2}{3}V_{dc}$	-$\frac{1}{3}V_{dc}$	$\frac{2}{3}V_{dc}e^{j\frac{4\pi}{3}}$
VI	1	1	0	V_{dc}	V_{dc}	0	0	V_{dc}	-V_{dc}	$\frac{1}{3}V_{dc}$	$\frac{1}{3}V_{dc}$	-$\frac{2}{3}V_{dc}$	$\frac{2}{3}V_{dc}e^{j\frac{5\pi}{3}}$
VII	0	0	0	0	0	0	0	0	0	0	0	0	0
VIII	1	1	1	V_{dc}	V_{dc}	V_{dc}	0	0	0	0	0	0	0

The eight base vectors are plotted on a hexagonal star diagram as shown in figure 2.5. The vectors V1 to V6 are known as the active vectors, while the vectors V0 and V7 are referred to as null vectors and are plotted at the origin of the star diagram.

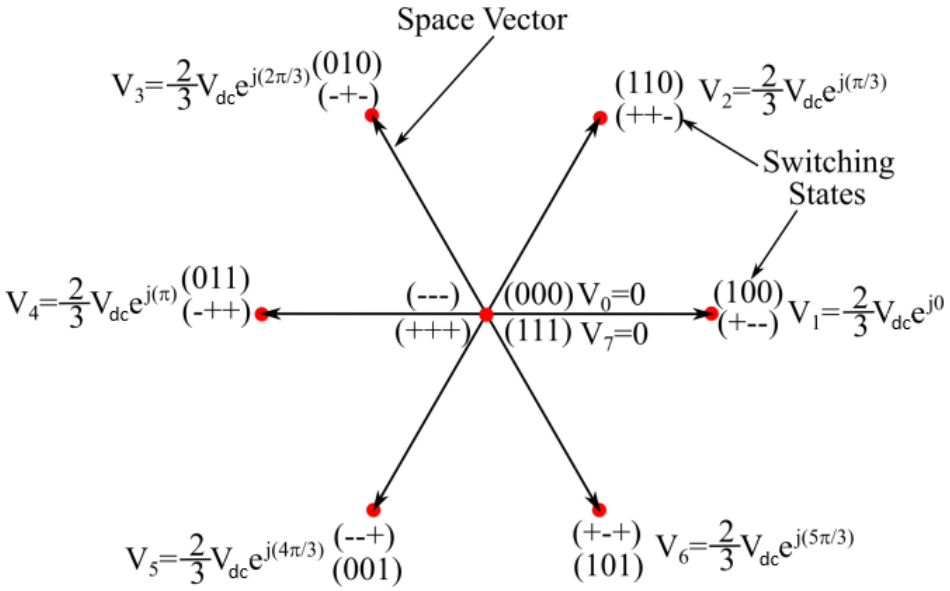

Figure 2.5: Space vector diagram

The location of v_r is determined on the star diagram. The active vectors that constrain that sector, along with one of the null vectors, are used to synthetize the desired voltage [14].

The space vectors are switched for a certain duration of time in a cycle to produce the resultant vector which can be expressed as:

$$v_r T_s = v_m T_1 + v_n T_2 + v_z T_0. \tag{2.37}$$

Where $v_{m,n}$ are the active vectors and v_z is one of the null vectors. T_0, T_1, T_2 are the switching time durations that can be calculated as follows:

$$T_1 = T_s \frac{\sqrt{3} v_r}{v_d} sin(\frac{n}{3}\pi - \theta) \tag{2.38}$$

$$T_2 = T_s \frac{\sqrt{3} v_r}{v_d} sin(\theta - \frac{n-1}{3}\pi) \tag{2.39}$$

$$T_0 = T_s - T_1 - T_2 \tag{2.40}$$

Where n = 1 to 6 [15]

The switching sequence is derived in terms of seven segments. Figure 2.6 shows how v_r passes through all 6 segments, and the table 2.2 represents different switching sequences in all six sectors of the SVPWM scheme [16].

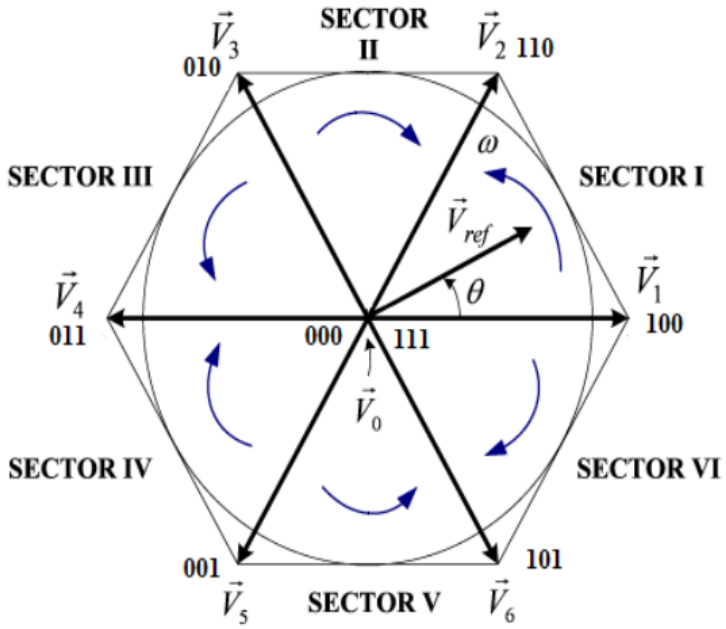

Figure 2.6: Space vector diagram with switching sequence

Table 2.2: Conventional Switching Sequence

Sectors	**Switching segments**						
	1	2	3	4	5	6	7
I	$\vec{V}_0$ [000]	$\vec{V}_1$ [100]	$\vec{V}_2$ [110]	$\vec{V}_0$ [000]	$\vec{V}_2$ [110]	$\vec{V}_1$ [100]	$\vec{V}_0$ [000]
II	$\vec{V}_0$ [000]	$\vec{V}_3$ [010]	$\vec{V}_2$ [110]	$\vec{V}_0$ [000]	$\vec{V}_2$ [110]	$\vec{V}_3$ [010]	$\vec{V}_0$ [000]
III	$\vec{V}_0$ [000]	$\vec{V}_3$ [010]	$\vec{V}_4$ [011]	$\vec{V}_0$ [000]	$\vec{V}_4$ [011]	$\vec{V}_3$ [010]	$\vec{V}_0$ [000]
IV	$\vec{V}_0$ [000]	$\vec{V}_5$ [001]	$\vec{V}_4$ [011]	$\vec{V}_0$ [000]	$\vec{V}_4$ [011]	$\vec{V}_5$ [001]	$\vec{V}_0$ [000]
V	$\vec{V}_0$ [000]	$\vec{V}_5$ [001]	$\vec{V}_6$ [101]	$\vec{V}_0$ [000]	$\vec{V}_6$ [101]	$\vec{V}_5$ [001]	$\vec{V}_0$ [000]
VI	$\vec{V}_0$ [000]	$\vec{V}_1$ [100]	$\vec{V}_6$ [101]	$\vec{V}_0$ [000]	$\vec{V}_2$ [110]	$\vec{V}_6$ [101]	$\vec{V}_0$ [000]

2.6 Modeling of Lithium-ion battery

An effective battery model is indispensable in designing important systems such as electric vehicles in order to accurately predict the electrical characteristics of the battery, including the voltage across it, the current flowing through it, and estimate the State of Charge (SOC, a normalized estimation of how much chemical energy is stored in a cell).

Figure 2.7 shows how a typical Li-ion cell reacts to a pulse of discharge current and a pulse of charge current.

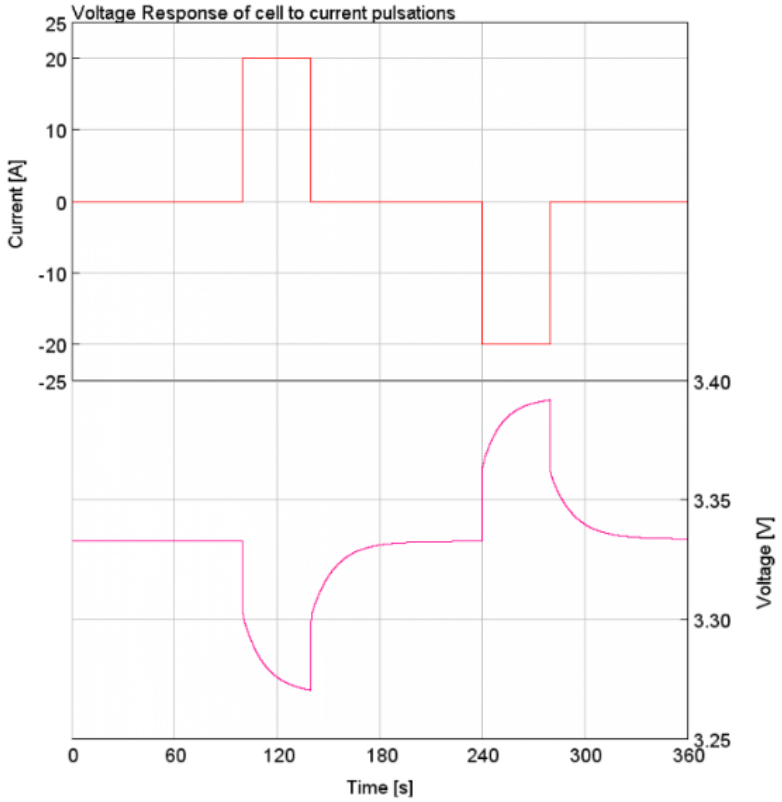

Figure 2.7: Voltage response of cell to current pulsations

In order to be able to capture the exponential decay behavior in the voltage response, one or multiple resistor-capacitor (RC) branches can be included in the electrical-equivalent model, referred to as a Thevenin battery model [17] as illustrated in figure 2.8. The resistive and capacitive characteristics of the battery mainly capacitive

impedance are raised from polarization phenomena and ohmic resistance of the battery [18].

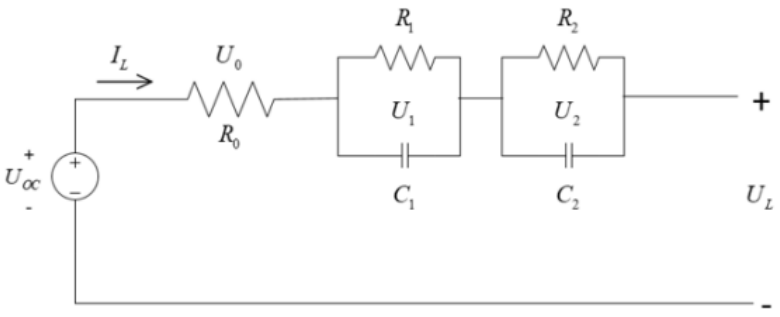

Figure 2.8: Thevenin battery model

2.7 Conclusion

This chapter has provided a detailed exploration of key components for electric vehicle systems. We covered the vehicle dynamics, the mathematical modeling of IPMSM in the stationary reference frame and the rotating reference frame. The voltage source inverter (VSI), the space vector pulse width modulation, and the modeling of a lithium-ion battery were also presented.

Chapter 3

System Control

3.1 Introduction

The ease of controlling electrical drives is an important aspect for meeting the increasing demands for flexibility and precision, for this purpose, various control systems have been developed [19]. IPMSM motors are typically controlled using field-oriented control scheme which provides good control capability over the full torque and speed ranges. MTPA is a novel technique that computes the d-axis and q-axis reference current values for maximum torque. Among more modern techniques, predictive control appears to be an interesting alternative to standard PI control like FOC. One of the best known predictive control schemes are deadbeat control and model predictive control.

3.2 Conventional Field Oriented Control

The AC motor control is rendered equivalent to that of the DC machine by a decoupling control known as vector control or field oriented control (FOC), which allows a precise control of torque and speed by decoupling the control of magnetic flux and electric torque components in the motor.

The control theory involves transforming the three-phase quantities of the motor from the stationary reference frame (abc) to a rotating reference frame (dq). In the rotating reference frame, the control of the q-axis current allows for precise control of the motor's torque, and the control of the d-axis current allows for precise control of the motor's magnetic flux.

FOC employs control algorithms, such as Proportional-Integral (PI) controllers, which are integrated to track the reference speed and current compared with the feedback values. The proportional component responds to the current error between the desired and actual motor state and adjusts the control signal proportionally to reduce the error. The integral component accumulates the historical error over time and eliminates any steady-state error, ensuring precise control and stability. It is worth knowing that tuning PI parameters for optimal performance can be challenging, and they may struggle with highly nonlinear or time-varying systems.

Feedforward compensation can be added to the current controller to improve the performance of our system by predicting and preventing disturbances in the input before they can affect the output. This control is based on the equations of voltage in the dq reference axis which gives the desired and predicted output regardless of the disturbances. It improves the energy efficiency, reduces harmonics, and enhances the system's stability. The schematic in figure 3.1 shows how to implement the feedforward compensation in our control.

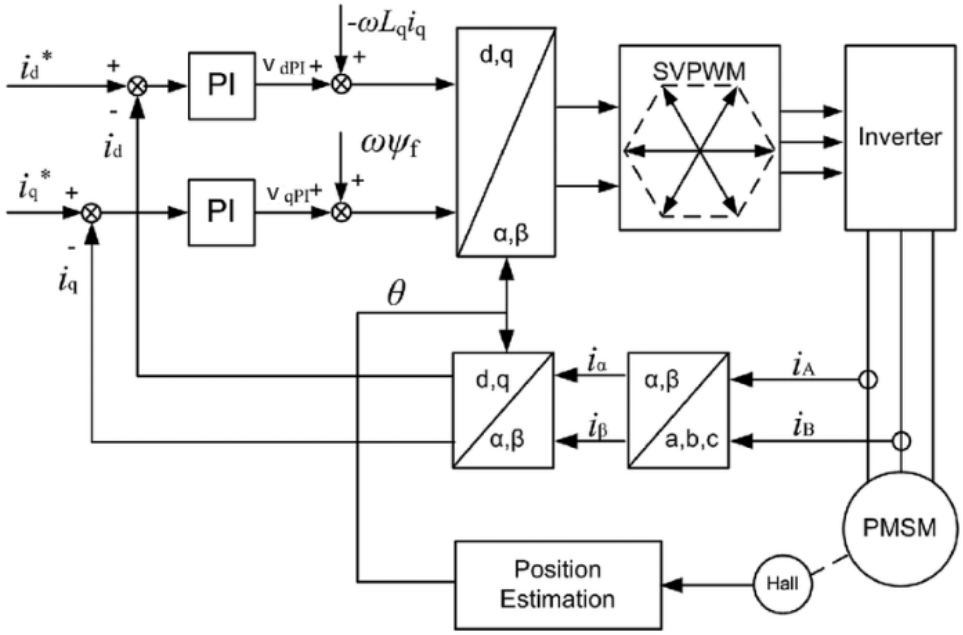

Figure 3.1: Field oriented control scheme with feedforward compensation

3.3 Maximum Torque Per Ampere Control

Maximum torque per ampere control is a technique employed with interior permanent magnet synchronous motors. It can minimize the electrical losses, enhance the motor's efficiency and reduce the risks of overheating. Additionally, the precise torque control enhances the motor's dynamic performance by ensuring a smooth and responsive torque delivery, improving acceleration and overall drive quality of EVs.

3.3.1 Control strategy of MTPA

The saliency of the rotor magnetic circuit in IPMSM causes an increased Lq/Ld ratio resulting in reluctance torque in the rotor. The maximum torque per ampere (MTPA) control utilizes the reluctance torque to generate more torque at lower operating speed.

It follows from 2.31 that the combination of id and iq that can yield a given torque is not unique. MTPA control operates by adjusting the current components in the dq axis reference frame to the most ideal combination in order to maximize the torque

which is influenced by both the direct axis and quadrature axis currents.

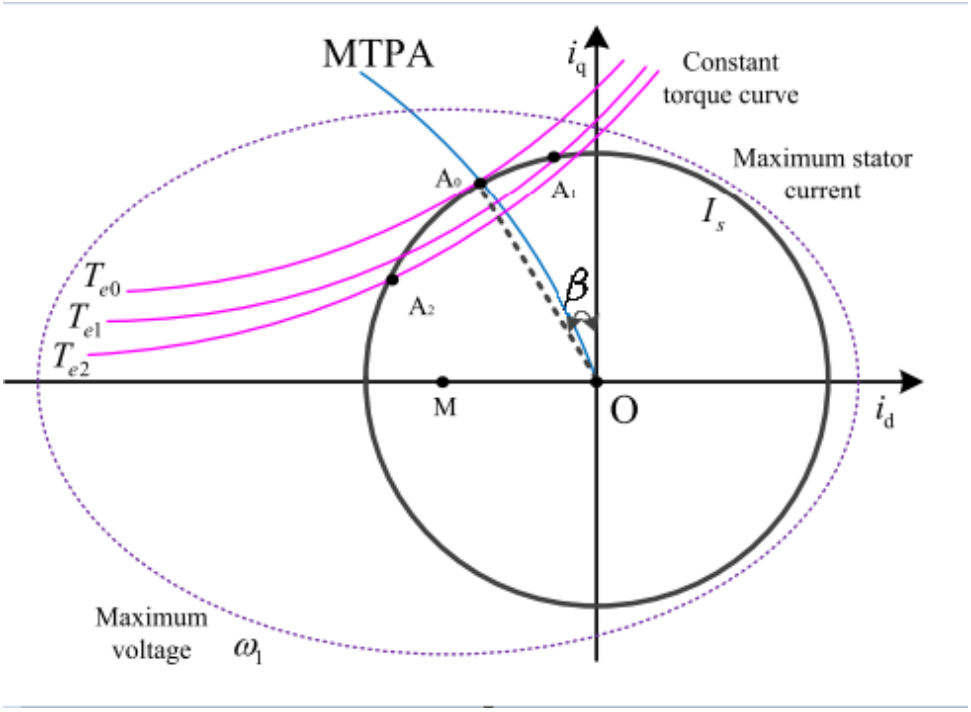

Figure 3.2: Stator current vector trajectory of MTPA

As can be seen from figure 3.2, the MTPA trajectory is the connection line of the maximum torque operating point corresponding to different stator current amplitudes. A_0, A_1 and A_2 are different combinations of d-axis current and q-axis current based on constant stator current amplitude Is. These combinations are all within the maximum voltage limiting range, and T_{e0}, T_{e1}, T_{e2} are the corresponding constant torque curves of each point respectively. Since the relationship between the torque value is $T_{e0} > T_{e1} > T_{e2}$, point A_0 can output the maximum torque under the same stator current amplitude [20].

According to figure 3.3, the relationship between d-axis current, q-axis current, electromagnetic torque, stator current amplitude, and current angle is shown in 3.1

and 3.2

$$\begin{cases} i_d = -I_s sin(\beta) \\ i_q = I_s cos(\beta) \end{cases} \tag{3.1}$$

$$T_e = \frac{3p}{2}[\lambda_{PM} I_s cos(\beta) - (L_d - L_q) I_s^2 sin(\beta) cos(\beta)] \tag{3.2}$$

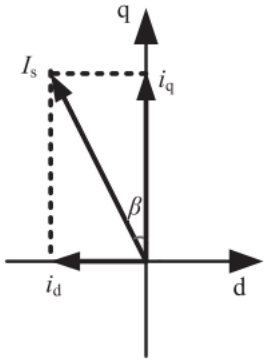

Figure 3.3: Relationship between I_s and d-q axis currents

It can be found that when the partial derivative of torque to the current angle is zero, the combination of d-axis and q-axis current is MTPA operating point. Therefore, at the MTPA operating point, the relationship between the electromagnetic torque and the stator current satisfies 3.4

$$\frac{dT_e}{d\beta} = 0 => \frac{3P}{2}[-\lambda_{PM} I_s sin(\beta) - (L_d - Lq) I_s^2 cos(2\beta)] = 0 \tag{3.3}$$

According to 3.3 and 3.2, the angle between the stator current vector and the q-axis at the MTPA operating point can be obtained as demonstrated below:

$$\beta = arcsin\left[\frac{-\lambda_{PM} + \sqrt{\lambda_{PM}^2 + 8(L_d - L_q)^2 I_s^2}}{4(L_d - L_q)}\right] \tag{3.4}$$

Substituting 3.4 in 3.1 and 3.2 yields to :

$$i_d = \frac{\lambda_{PM}}{2(L_q - L_d} - \sqrt{\frac{\lambda_{PM}^2}{4(L_q - L_d)^2} + i_q^2} \tag{3.5}$$

$$i_{qref} = (L_q - L_d)^2 * i_q^4 + \frac{2T_e}{3p}\lambda_{PM} i_q - (\frac{2T_e}{3p})^2 \tag{3.6}$$

By solving equation 3.6 using Newton-Raphson and substituting it in the torque equation 3.4 yields to the reference value i_d for MTPA operation [21].

$$i_{dref} = \frac{2T_e}{3pi_{ref}(L_d - L_q)} - \frac{\lambda_{PM}}{(L_d - L_q)} \tag{3.7}$$

3.4 Predictive control

Predictive control covers a very wide class of controllers that have found rather recent application in power converters and drives. A classification for different predictive control methods is shown in figure 3.4.

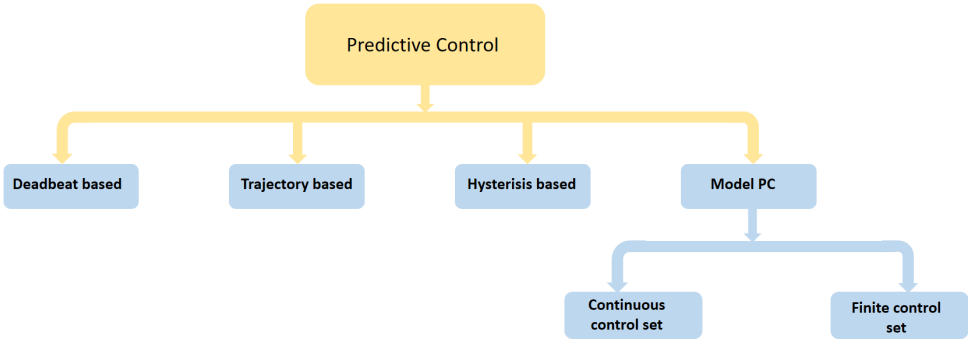

Figure 3.4: Classification of predictive control methods

Predictive controllers use models of the system to create predictions of future states and variables to control. With this information the actuation in the system is obtained according to the method used.

- Hysterisis based predictive control keeps the controlled variable within boundaries of a hysteresis area. It needs no modulator. It calculates the instant the switching states must change. Thus it requires a variable frequency.

- Trajectory based predictive control forces the controlled variables to follow a predefined trajectory. It calculates the different optimum control strategies based in different states and applies them directly. This control does not need

a cascaded control as the speed can be controlled directly from the speed error. Since the instants at which the switching states change are calculated, variable frequency is needed.

– Deadbeat based predictive control generates the optimal actuation which makes the speed error equal to zero in the next sampling instant. It uses a modulator and fixed frequency.

– Model predictive control can use modulators and fixed switching frequency which is known as continuous control set or a finite control set where different switching states are tried within a horizon. A cost function with the errors between variables is created and optimized by modifying the different control variables through an optimization algorithm [22, p. 1–2] [3, p. 32].

Table 3.1 summarizes the characteristics of the different control types [23]

Table 3.1: Predictive controller types

	Model Predictive Control (MPC)		
	Continuous Control Set	Finite Control Set	Deadbeat Control
Switching Frequency Sensitivity	Yes	No	Yes
Sensitivity of Model parameters	Medium	Bad	Good
Stress level on the inverter	Medium	Good	Bad
Computation requirement	Bad	Bad	Good
Constraint Implementation	Yes	Yes	No

3.4.1 Deadbeat control

Deadbeat control is a control strategy used in various applications such as power electronics, motor drives, and process control. Deadbeat control predicts the future

behavior of the system based on its current state and a mathematical model that includes the system's dynamics. Using this prediction, the control input is calculated to bring the system output to the desired value by the next sampling instant.
The deadbeat controller scheme can be seen in figure 3.5. It replaces the PI of the current controller used in conventional field oriented control shown in figure 3.1. The machine voltages are generated using the SVPWM block to control the inverter. This guarantees a fixed switching frequency.

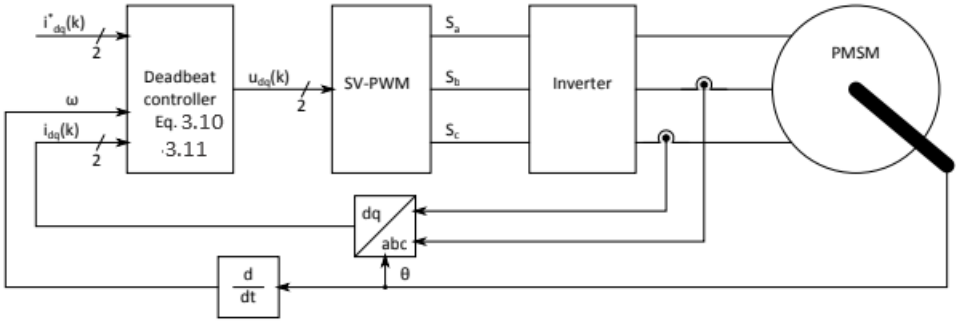

Figure 3.5: Deadbeat predictive control scheme

The deadbeat control algorithm is based on the IPMSM model. By discretizing the model, the voltage required to obtain the desired current vector i^*_{dq}(k) at the next sampling instant can be obtained. The electrical machine model equations 2.29 and 2.30 can be discretized and thereby approximated using Newton's forward difference quotient as shown in 3.8 and the average equation for the next period as shown in 3.9 by assuming a fixed sampling time approaching zero.

$$\frac{di_{dq}(t)}{dt} = \frac{i_{dq}(k+1) - i_{dq}(k)}{T_s} \tag{3.8}$$

$$i_{dq}(t) = \frac{i_{dq}(k+1) + i_{dq}(k)}{2} \tag{3.9}$$

By substituting the derivatives in 2.29 and 2.30, rearranging for the currents at the next sampling instant and by assuming that $i^*_{dq}(k) = i_{dq}(k+1)$ since the desired current is the reference one, the necessary discretized model is obtained as shown in

3.10 and 3.11.

$$v_q(k+1) = R\frac{i_q^*(k) + i_q(k)}{2} + L_q\frac{i_q^*(k) - i_q(k)}{T_s} + w_e(k)(L_d\frac{i_d^*(k) + i_d(k)}{2} + \lambda_{PM}) \quad (3.10)$$

$$v_d(k+1) = R\frac{i_d^*(k) + i_d(k)}{2} + L_d\frac{i_d^*(k) - i_d(k)}{T_s} - w_e(k)L_q\frac{i_q^*(k) + i_q(k)}{2} \quad (3.11)$$

Where ω_e is the rotor electrical speed (given by the product of the number of pole pairs p and the the mechanical speed ω_r).

By assuming $i_{dq}^*(k) - i_{dq}(k) = 0$ at sampling instant k it can be seen that the reference voltages need not change in the next sampling instant since the speed voltages are constant. The deadbeat control method functions as a kind of high gain proportional controller if the rotor speed and back-EMF terms are compensated properly [22, p. 27].

3.4.2 Finite control set Model predictive control strategy (FCS-MPC)

Model predictive control is a control technique increasingly used in EV motors for its ability to optimize performance while accounting for constraints and uncertainties. MPC relies on a dynamic model of the motor system to predict its future behavior based on current inputs and system states. This model accounts for motor dynamics, constraints and external disturbances. MPC formulates an optimization problem to minimize a cost function that captures desired performance criteria, such as maximizing torque efficiency subject to system constraints.

Considering the finite number of switching states and fast micro-processors available today, calculation of the optimal actuation by online evaluation of each switching state is possible to implement in real systems. This consideration allows more flexibility and simplicity in the control scheme[3, p. 35]. Figure 3.6 shows the finite control set model predictive control scheme.

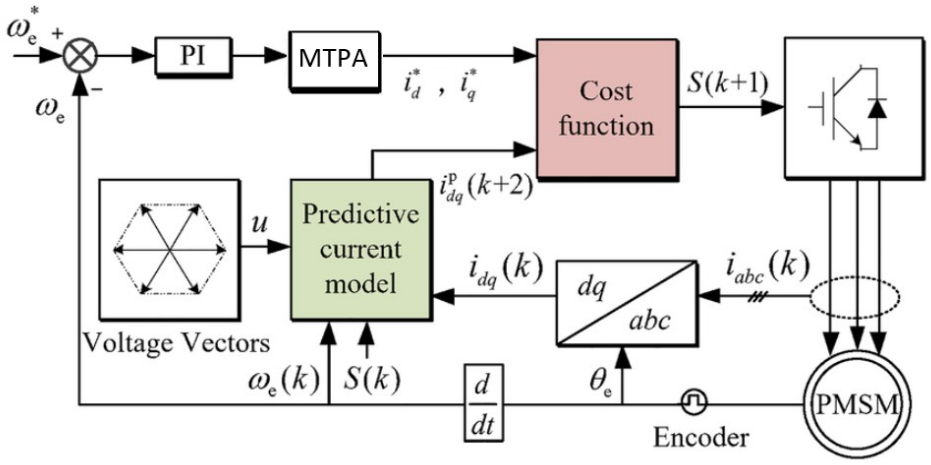

Figure 3.6: Finite Control Set Model Predictive Control scheme

In order to predict the system's behavior at each switching state, the discretized model of IPMSM is necessary.

Reordering equations 2.29, 2.30 and 2.32 gives:

$$\frac{di_d}{dt} = \frac{1}{L_d}(v_d - Ri_d + \omega_e(k)L_q i_q) \tag{3.12}$$

$$\frac{di_q}{dt} = \frac{1}{L_q}(v_q - Ri_q - \omega_e L_d i_d - \omega_e \lambda_{PM}) \tag{3.13}$$

$$\frac{d\omega_e}{dt} = \frac{p}{J}(T_{em} - \frac{B}{p}\omega_e - T_L) \tag{3.14}$$

The forward Euler discretization technique is employed with a sampling interval T_s to the system above.

$$i_d(k+1) = i_d(k) - T_s N_1 i_d(k) + T_s N_2 v_d(k) + T_s N_3 \omega_e i_q(k) \tag{3.15}$$

$$i_q(k+1) = i_q(k) - T_s N_4 i_q(k) + T_s N_6 v_q(k) - T_s N_7 \omega_e(k) i_d(k) - T_s N_5 \omega_e(k) \tag{3.16}$$

$$\omega_e(k+1) = \omega_e(k) + T_s N_8 i_q(k) - T_s N_9 \omega_e(k) - T_s N_{10} T_L(k) + T_s N_{11} i_d(k) i_q(k) \tag{3.17}$$

Where the model parameters $N_\delta(\delta$=1,2....11) are defined as:

$$N_1 = \frac{R}{L_d},\quad N_2 = \frac{1}{L_d},\quad N_3 = \frac{L_q}{L_d},\quad N_4 = \frac{R}{L_q},\quad N_5 = \frac{\lambda PM}{L_q},\quad N_6 = \frac{1}{L_q},\quad N_7 = \frac{L_d}{L_q}$$

$$N_8 = \frac{1.5\lambda_{PM}p^2}{J}, \quad N_9 = \frac{B}{J}, \quad N_{10} = \frac{p}{J}, \quad N_{11} = (\frac{1.5p^2}{J})(L_d - L_q)$$

The proposed control predicts the future behaviors of the manipulated states for all possible switching states in every sampling interval. The future dq-axis stator currents are obtained by computing 8 stator current predictions.

$$\tilde{i_d}(k+2) = (1 - T_s N_1) i_d(k+1) + T_s N_2 v_d(k+1) + T_s N_3 \omega_e(k+1) i_q(k+1) \quad (3.18)$$

$$\tilde{i_q}(k+2) = (1 - T_s N_4) i_q(k+1) + T_s N_6 v_q(k+1) - T_s N_7 \omega_e(k+1) i_q(k+1) - T_s N_5 \omega_e(k+1) \quad (3.19)$$

The '$\sim$' denotes the predicted estimate.

The control signals in the above equations are obtained as follows:

$$v_{dq}(k+1) = \begin{bmatrix} v_d(k+1) \\ v_q(k+1) \end{bmatrix} = (\frac{2}{3} V_{dc}) M^T \begin{bmatrix} S_a(k+1) \\ S_b(k+1) \\ S_c(k+1) \end{bmatrix} \quad (3.20)$$

Where M(k) is a rotational transformation matrix defined as [24]

$$M(k) = \begin{bmatrix} cos(\theta_e(k)) & -sin(\theta_e(k)) \\ cos(\theta_e(k) - \frac{2\pi}{3}) & -sin(\theta_e(k) - \frac{2\pi}{3}) \\ cos(\theta_e(k) + \frac{2\pi}{3}) & -sin(\theta_e(k) + \frac{2\pi}{3}) \end{bmatrix} \quad (3.21)$$

Because the sampling period is quite short, the variation in θ_e between the (k+1)th instant and the kth instant is neglected The switching parameters are given as:

$$\begin{cases} S_{abc}(k+1) \in \{S_a(k+1), S_b(k+1), S_c(k+1)\} \\ S_{abc}(k+1) \in \{000, 100, 110, 010, 011, 001, 101, 111\} \end{cases} \quad (3.22)$$

Similarly, the corresponding cost function results related to the eight stator current predictions are evaluated to determine an optimal switching state that minimizes

the prediction errors of the stator currents. The cost function equation for the proposed FCS-MPC scheme is represented as: [25]

$$\tilde{\Pi} = (i_d^* - \tilde{i_d}(k+2))^2 + (i_q^* - \tilde{i_q}(k+2))^2 \tag{3.23}$$

3.5 DC-DC converter

DC-DC converters are essential electronic circuits that play a crucial role in battery management systems. They convert the voltage of a direct current (DC) source from one level to another (magnitude and sometimes polarity), ensuring stable and efficient power delivery to various electronic devices and systems. In applications where input voltage levels can fluctuate due to factors such as battery discharging over time or changes in load conditions, DC-DC converters maintain a constant output voltage, providing reliable power to the system's components.
The dc–dc converters are implemented by the use of diodes, LC circuits as well as semiconductors like insulated gate bipolar transistors (IGBTs), power metal-oxide-semiconductor field effect transistors (MOSFETs) and thyristors which operate as switches. These controlled semiconductor devices are operating only in the conduction state or in the blocking state. If a gating pulse is applied to the gate of an IGBT or MOSFET, then they will be switched into the conduction mode and will remain in this state until the end of the gating pulse interval. When the gating pulse becomes zero, the semiconductor devices are switched into blocking mode. These switching techniques minimize power losses associated with resistive elements which typically generate heat and waste energy, this results in better overall efficiency and prolonged battery life [26]. DC-DC converters also offer the flexibility to step up or down voltage levels, allowing for efficient power distribution management.

3.5.1 Principle of operation of half-bridge bidirectional DC-DC converters

Energy stored in batteries is transferred to motor via DC–DC converter in the normal motoring operation. In this case, the DC–DC converter operates as a boost converter to boost battery terminal voltage to inverter's input voltage level and the battery pack is in discharging mode. Consequently, during the regenerative mode of operation, DC–DC converter acts as a buck converter. The energy from the motor is transferred back to the source and is used to charge batteries. The proposed block diagram of DC–DC converter along with a two-level inverter is shown in figure 3.7.

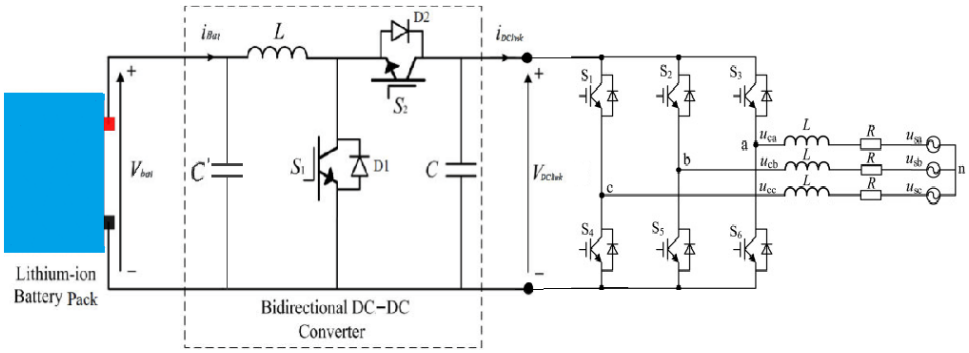

Figure 3.7: Half-bridge bidirectional converter scheme

The following sections explain the mode of operation of the DC-DC converter

- Boost mode: This mode is divided into two intervals. During the first interval namely the switch-on state, the switch S_1 is on while switch S_2, diode D1 and D2 are all off, the current will flow from the battery to the inductor which will store energy in its magnetic field and its current will increase linearly.

  During the second interval known as the switch-off state, the switch S_1 is turned off and only the diode D2 is on which leads to the release of the energy previously stored to the output. The current flows through the inductor,

output capacitor and the inverter.

Figure 3.8 illustrates both intervals for the boost mode.

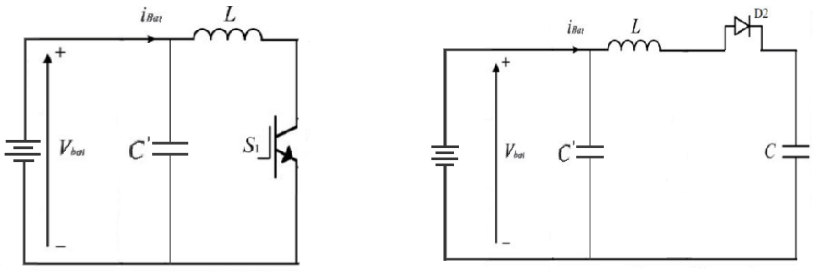

(a) First interval (b) Second interval

Figure 3.8: Boost mode's intervals

The relationship between the duty cycle (D) and the output voltage is given by:

$$V_{out} = \frac{V_b}{(1-D)} \tag{3.24}$$

with $D = \frac{T_{on}}{T}$ where T is the total switching period and T_{on} is the switch-on time.

- Buck mode: This mode is divided into two intervals. During the switch-on state, switch S_2 is on while switch S_1 and the diodes D1 and D2 are off. The current will flow through the inductor and the load.

  During the switch-off state, switch S_2 is off and only diode D1 is on. The energy stored in the inductor is release to the load.

  The output voltage is given by:

$$V_{out} = DV_b \tag{3.25}$$

The following figure shows both intervals for the buck mode [27].

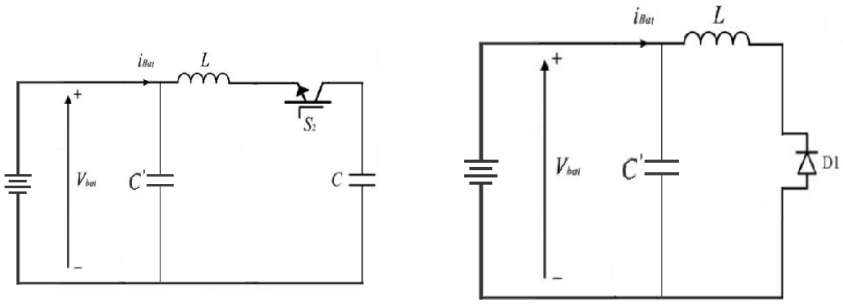

(a) First interval (b) Second interval

Figure 3.9: Buck mode's intervals

3.5.2 Control strategy for buck-boost converter

The control strategy of DC-DC converter in buck-boost modes are shown in figure 3.10.

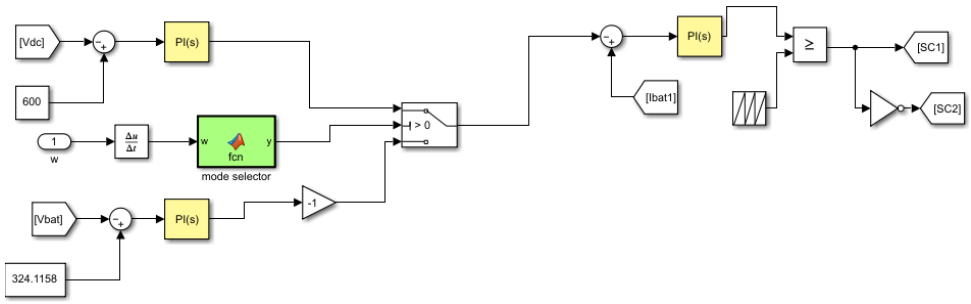

Figure 3.10: Half-bridge bidirectional converter control system

In driving mode, the energy needed to drive the electric motor is drawn from the battery pack, hence the batteries are in discharging mode and the converter is in boost mode. In order to generate the switching pulses for S_1 and S_2, DC link voltage is compared to its reference value and the output is processed through a PI controller, which is then compared to the battery current. The error is processed through a PI controller and compared with a high frequency triangular wave to generate desired pulses.

In regenerative mode, the kinetic energy is converted into electrical energy and is fed back to batteries; thus, battery bank is in charging state and the converter is

in buck mode. In order to generate the switching pulses for S_1 and S_2, battery voltage is compared to its reference value and the output is processed through a PI controller, which is then compared to the battery current. The error is processed through a PI controller block and compared with a high frequency triangular wave to generate desired pulses.

The flowchart below explains the mode selection [28].

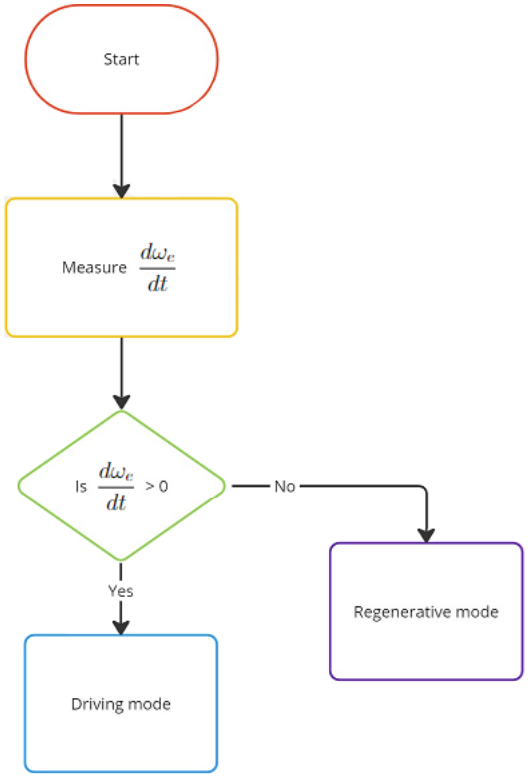

Figure 3.11: Flowchart for mode selection of DC-DC converter

3.6 Conclusion

Different control strategies for IPMSMs are proposed in this chapter. Field oriented control allows for precise speed and torque control. Maximum torque per Ampere delivers the maximum electromagnetic torque with the lowest current magnitude in order to enhance the motor efficiency. Predictive control creates predictions of future states and variables to control; deadbeat control sets the error equal to zero in the next sampling instant while the finite control set minimizes a cost function. Predictive control can easily include constraints and non-linearities present in the system. This chapter also covers bidirectional DC-DC converter with its control system.

Chapter 4

Simulation and Results

4.1 Introduction

In order to test the control systems studied above, several simulations were run using matlab/simulink software.

4.2 Motor parameters

The parameters of the IPMSM used in the simulations are presented in the table 4.1

Table 4.1: Motor parameters

Parameter	**Value**
Rated Power	9.42 kW
Rated DC link voltage	400 V
Stator resistance	0.25 Ω
d-axis inductance	2.03 mH
q-axis inductance	2.15 mH
PM Flux linkage	0.12 Wb
Inertia	2.03 kg m^2
Viscous friction coefficient	0.000456
Pole pairs	4

4.3 Simulation of FOC with MTPA with constant reference speed

Figure 4.1 shows the simulation model for the control of IPMSM using the FOC with MTPA supplied by a 400V DC voltage source.

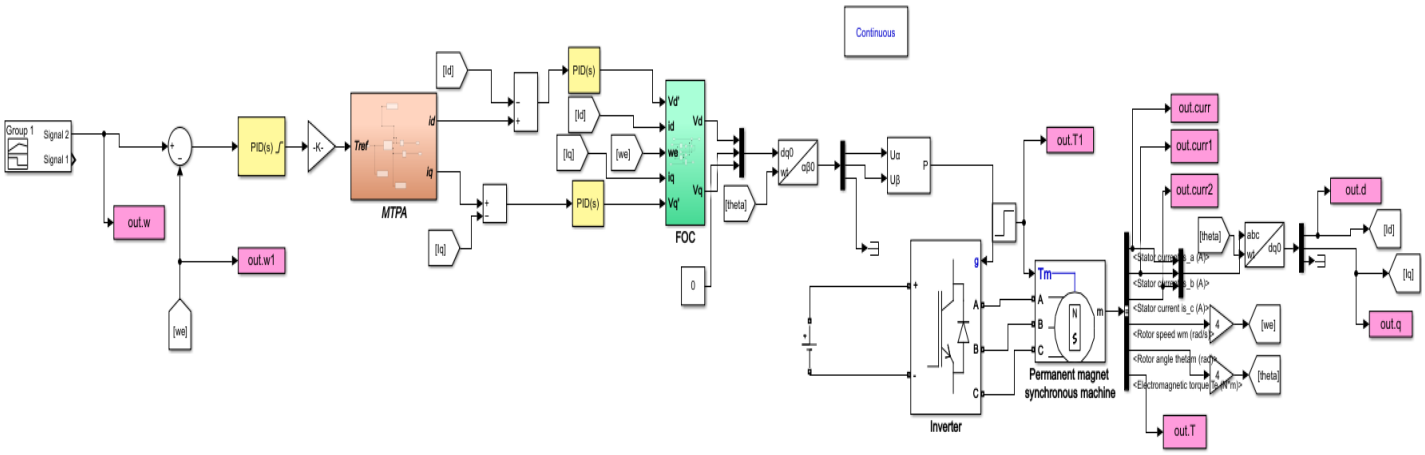

Figure 4.1: FOC with MTPA controlling IPMSM

The parameters for the PI controllers are shown in table 4.2.

Table 4.2: Parameters of PI controllers

Controlled signal	**Proportional gain(Kp)**	**Integral gain (Ki)**
Speed (ω)	20	0.2
Current ($\imath_{dq}$)	20	0.8

After simulating the model, the output signals are illustrated as follows:

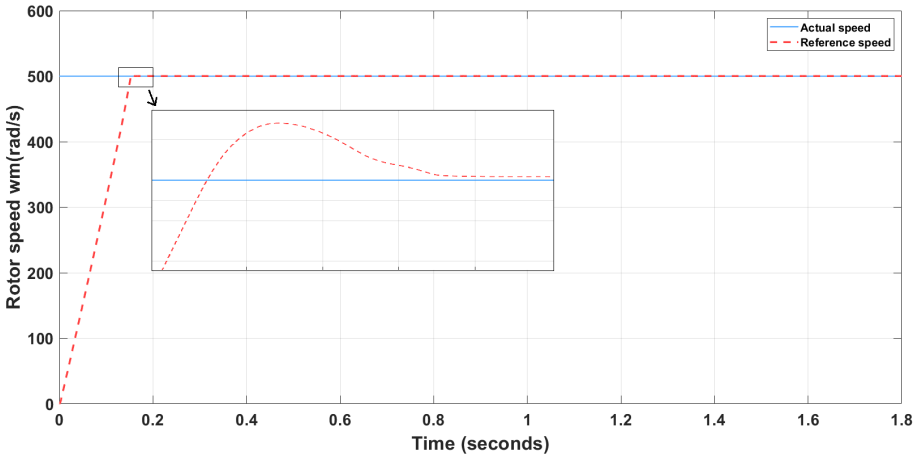

Figure 4.2: Speed response

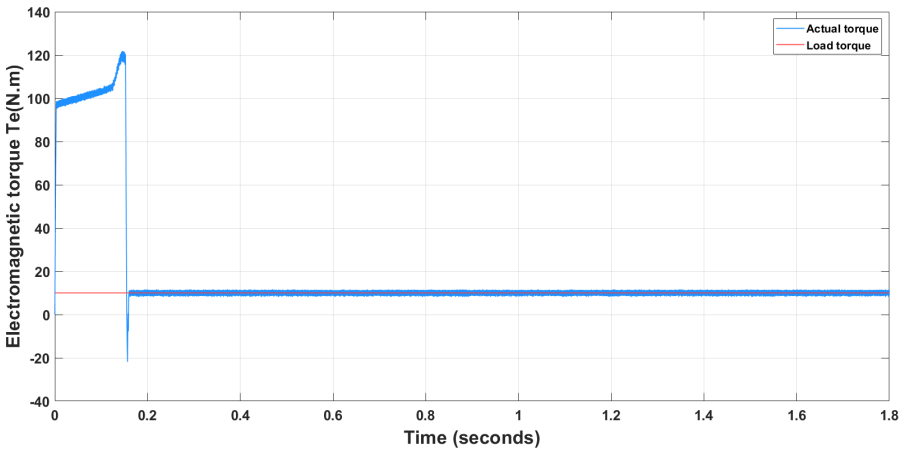

Figure 4.3: Torque response

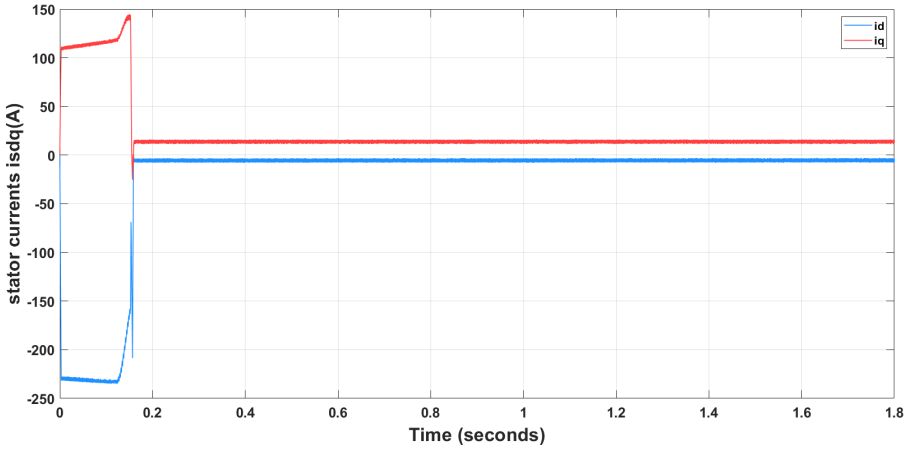

Figure 4.4: dq-axis components of stator currents

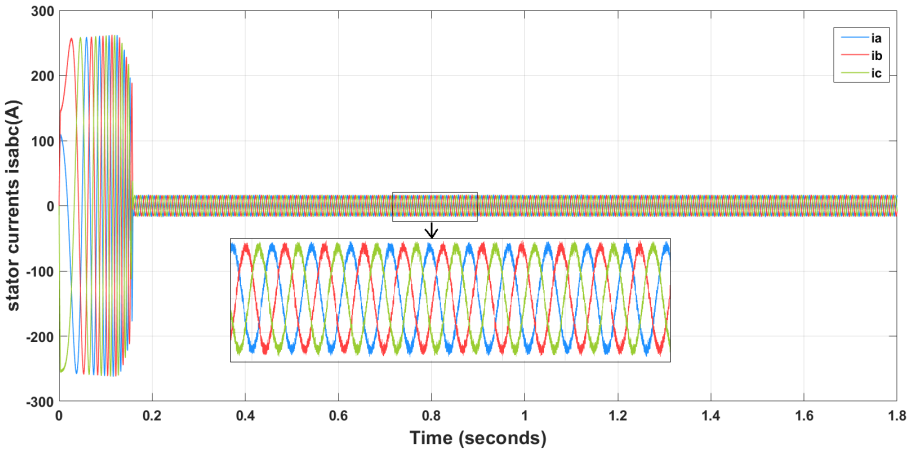

Figure 4.5: Stator currents

Figure 4.2 shows the speed response. The motor takes approximately 0.15s to go from no speed to 500rad/s.

As can be shown in figure 4.3 the motor requires a high starting torque to overcome the inertia and reach the reference speed. After reaching such a speed, the motor does not need as much torque to maintain its momentum, and thus the output torque remains at the level of the load torque.

Figure 4.4 shows the dq-axis components of the stator currents. The q-axis current is directly controlled to achieve the desired output torque which is why the output torque is directly proportional to iq. The d-axis current is negative or zero due to the optimization of torque production (MTPA) and efficiency of the system.

Figure 4.5 reveals that the stator current follows the same rate as the load torque.

4.4 Simulation of FOC with MTPA with variable reference speed

The same model and PI parameters were used as the previous simulation. However the reference speed was changed to be a variable one.

After simulating the model, the output signals are illustrated as follows:

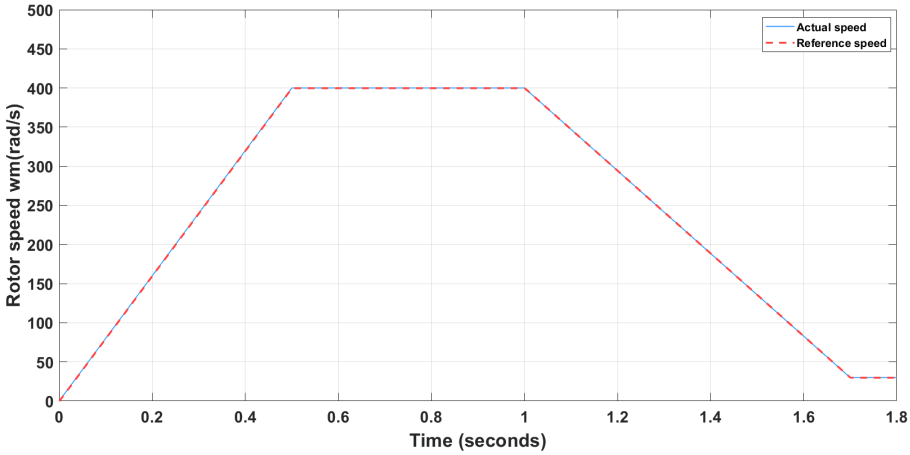

Figure 4.6: Speed response

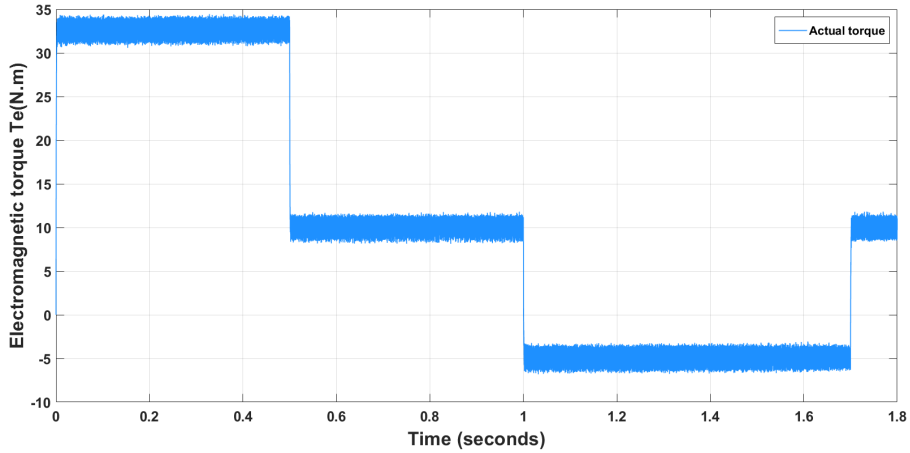

Figure 4.7: Torque response

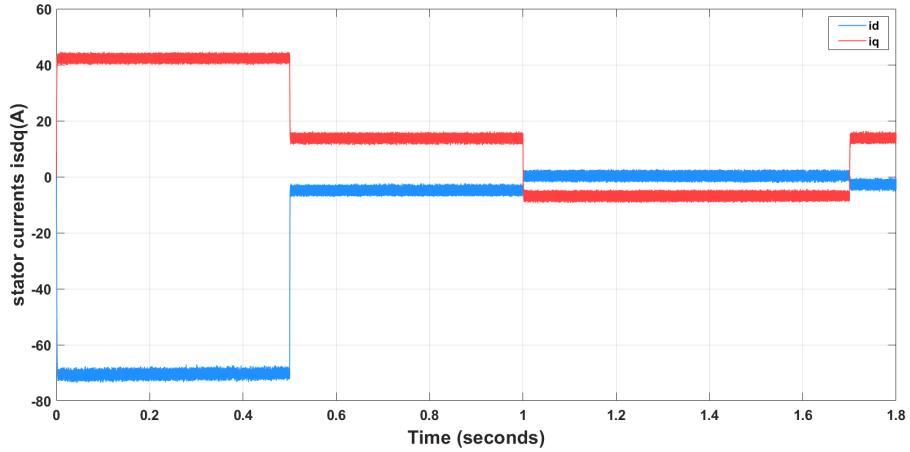

Figure 4.8: dq-axis components of stator currents

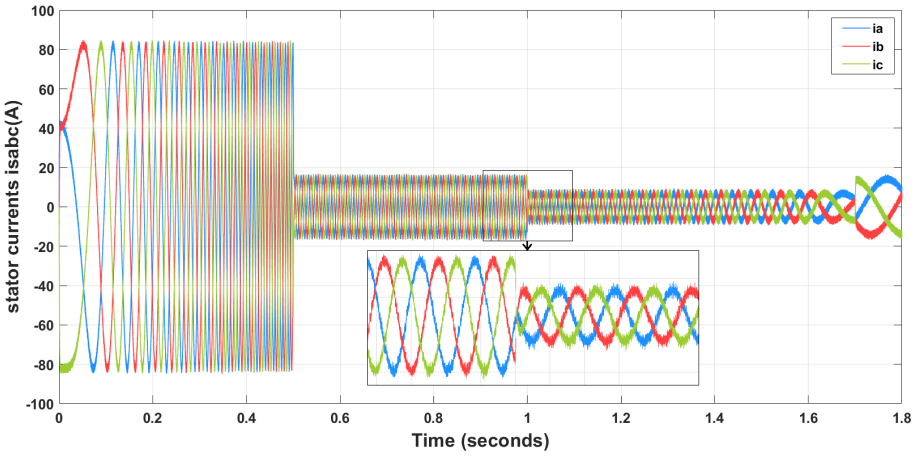

Figure 4.9: Stator currents

Figure 4.6 shows actual rotor speed along with the reference speed. As it can be seen, the rotor's speed is perfectly following the reference speed.

Figure 4.7 demonstrates the change in torque of the motor; the change in torque is related to the change in speed. From [0s to 0.5s] the torque is increased due to the motor's acceleration. As the speed becomes constant the torque decreases. From [1s to 1.7s] the torque is negative as a result of the deceleration. When the speed settles back, more torque is needed and so it increases.

Figure 4.9 shows the input currents of the motor. It is visible that the currents have some ripples and harmonics that may slightly affect the motor.

4.5 Simulation of deadbeat control with MTPA

Figure 4.10 shows the simulation model for the control of IPMSM using deadbeat control with MTPA, supplied by a 400V DC voltage source.

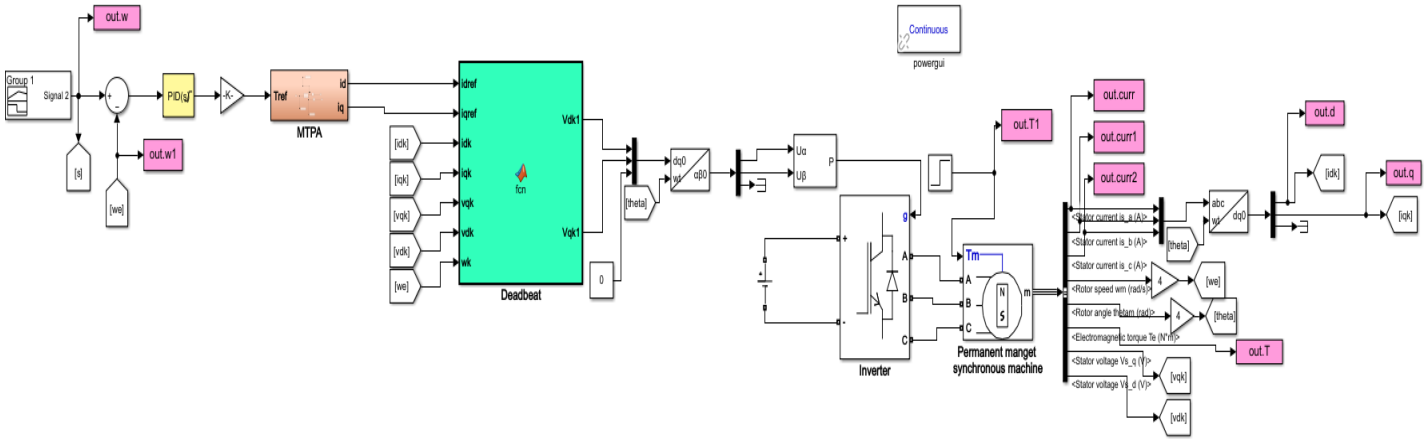

Figure 4.10: Deadbeat control with MTPA controlling IPMSM

The PI parameters for the speed loop are set as follows:

Sampling period Ts is set to 20μs.

Table 4.3: Parameters of PI controllers

Controlled signal	**Proportional gain(Kp)**	**Integral gain (Ki)**
Speed (ω)	10	0.001

After simulating the model, the output signals are illustrated below:

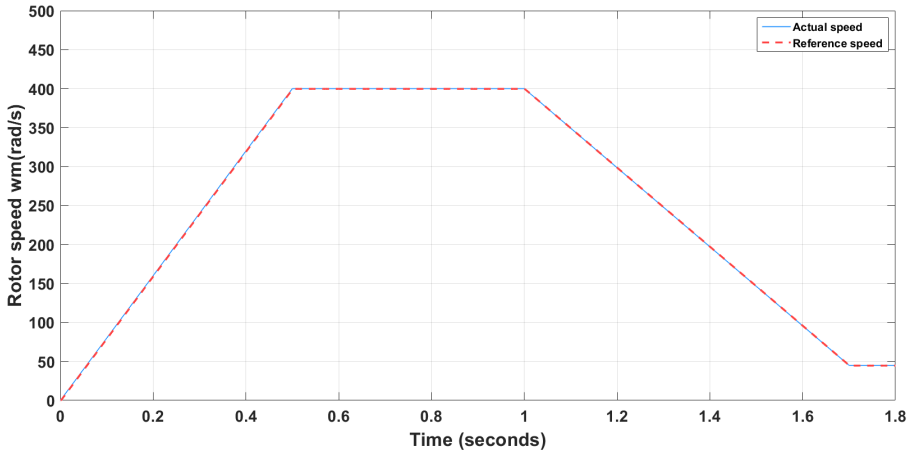

Figure 4.11: Speed response

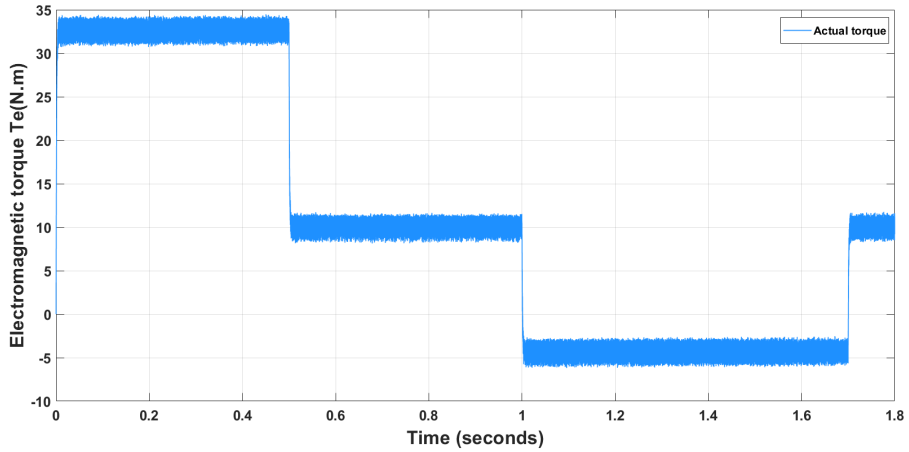

Figure 4.12: Torque response

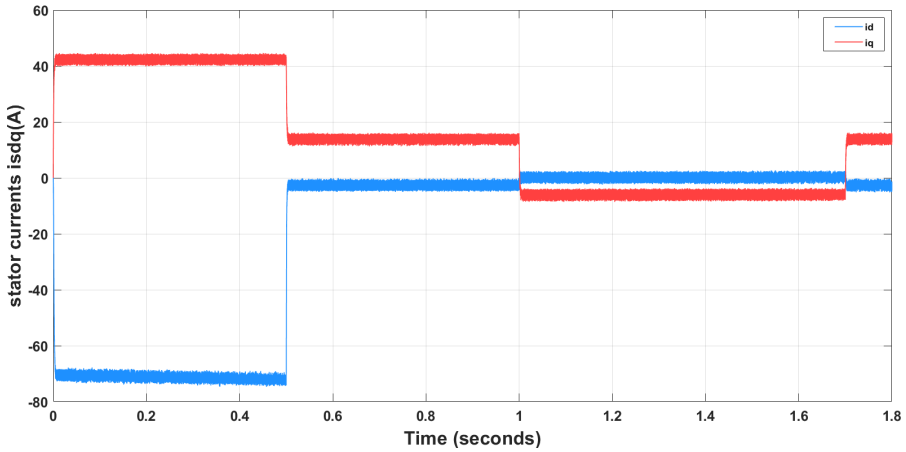

Figure 4.13: dq-axis components of stator currents

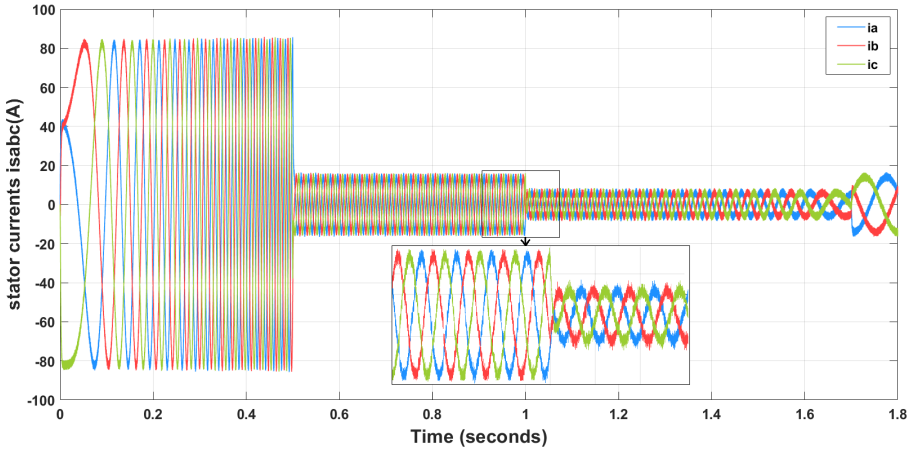

Figure 4.14: Stator currents

The figures 4.12, 4.13, and 4.14 show respectively the torque response, dq-axis components and input currents of the motor. In comparison to the FOC, the dead-beat control eliminates the overshoot during the change in speed. We can also notice

less harmonics and ripples in the signals.

4.6 Simulation of MPC with MTPA

Figure 4.15 shows the simulation model for the control of IPMSM using the MPC with MTPA, supplied by a 400V DC voltage source.

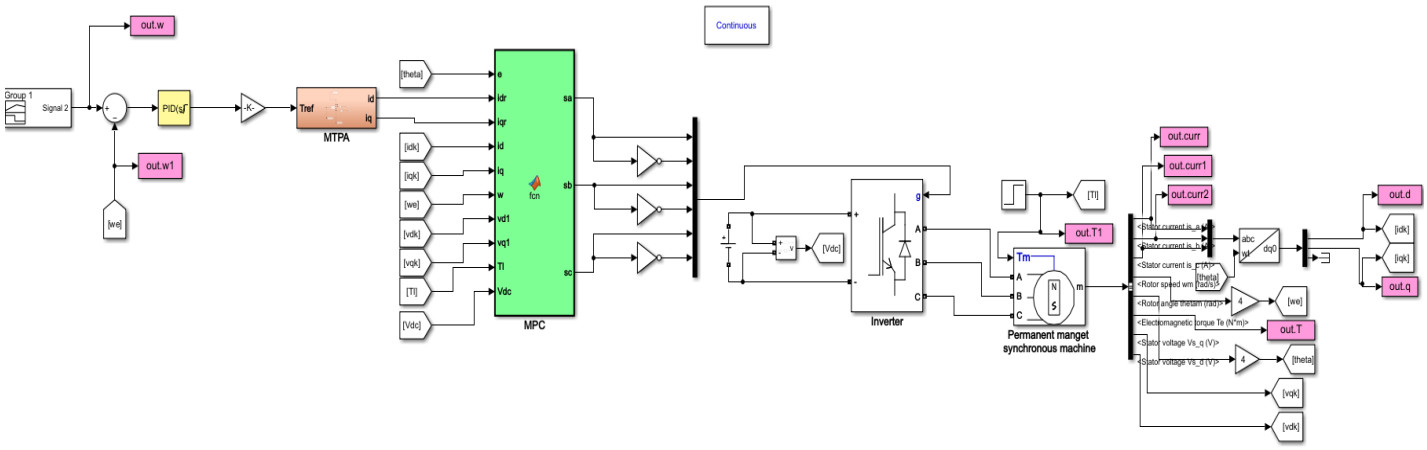

Figure 4.15: MPC with MTPA controlling IPMSM

Sampling period Ts is set to 58μs.

A more detailed description of the Matlab function code is found in Appedix A.

The PI parameters for the speed loop are set as follows:

Table 4.4: Parameters of PI controllers

Controlled signal	**Proportional gain(Kp)**	**Integral gain (Ki)**
Speed (ω)	5	0.001

After simulating the model, the output signals are illustrated as follows:

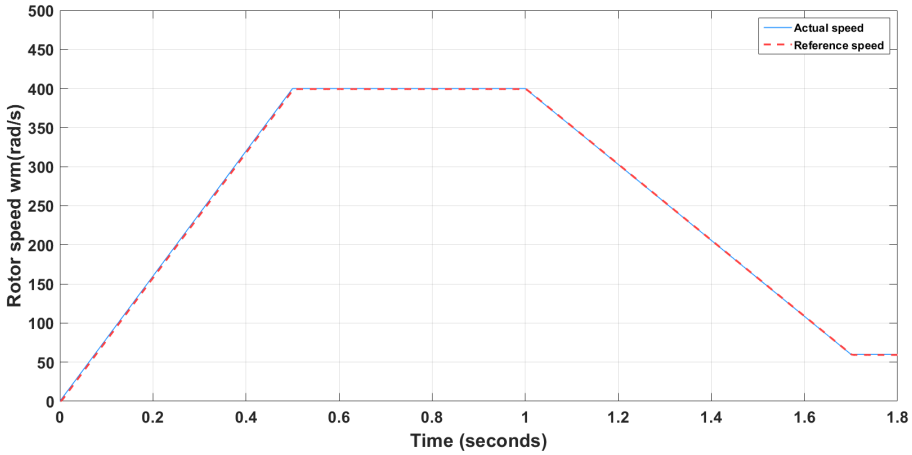

Figure 4.16: Speed response

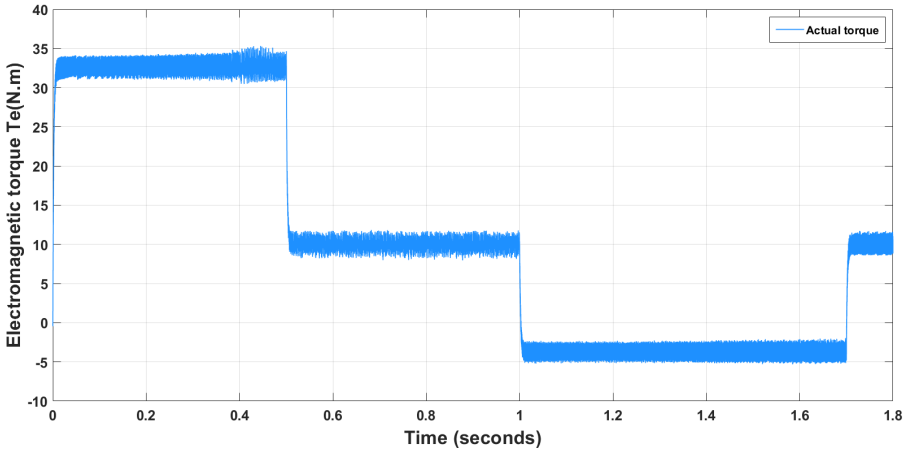

Figure 4.17: Torque response

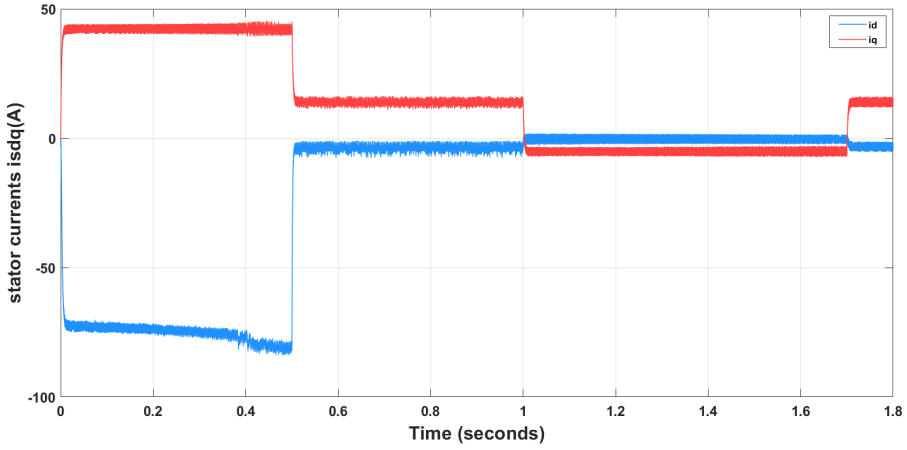

Figure 4.18: dq-axis components of stator currents

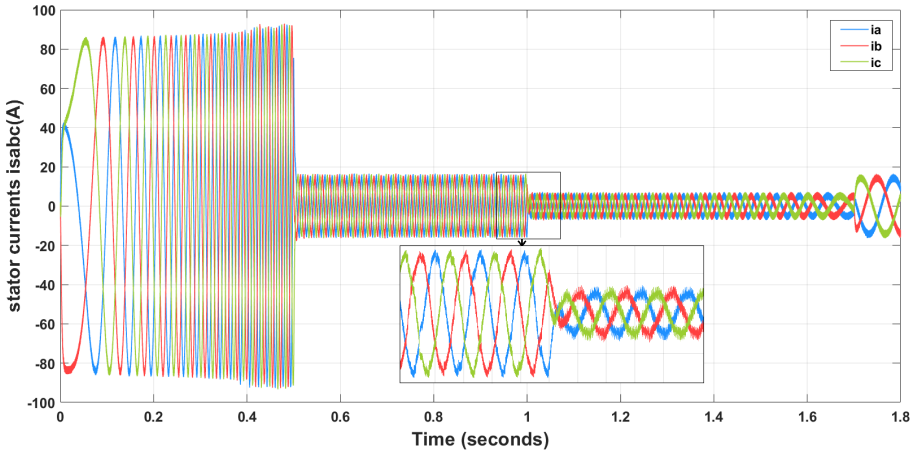

Figure 4.19: Stator currents

We can notice slightly more ripples and an overshoot in the output torque and dq currents in comparison to the deadbeat control, since the control system is more complex. The time response, however, for the MPC is significantly faster, owing to the absence of a pulse modulator.

4.7 Simulation of deadbeat control with MTPA connected to batteries

4.7.1 Without DC-DC converter

Figure 4.20 shows the simulation model for the control of IPMSM using the deadbeat control with MTPA, supplied by a 10×48V battery pack.

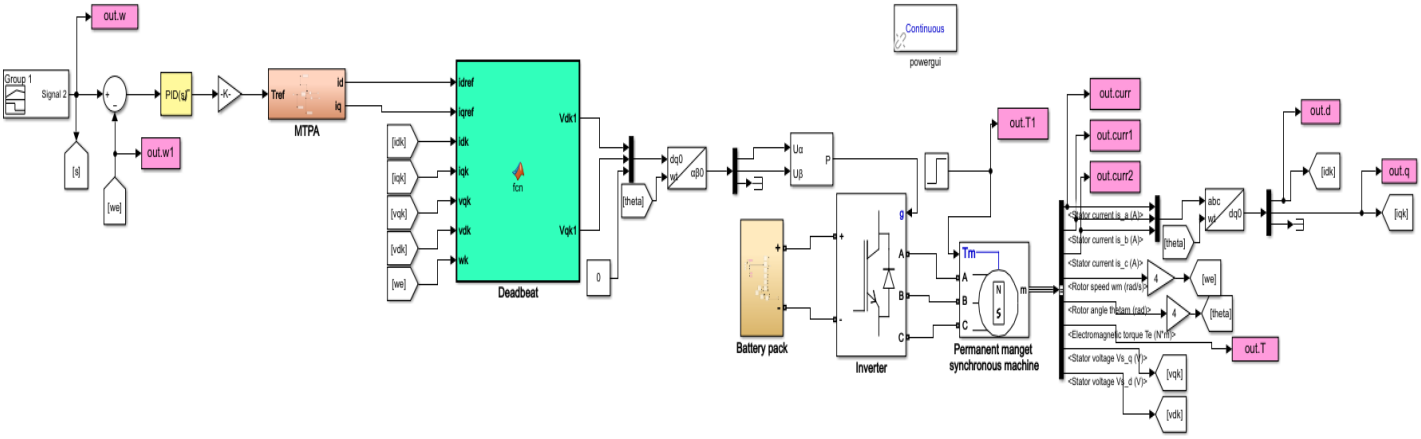

Figure 4.20: Deadbeat control with MTPA controlling IPMSM with battery pack

The battery characteristics are described in the table 4.5.

Table 4.5: Battery characteristics

Parameter	**Value**
Nominal voltage	48 V
Rated capacity	120 Ah
Cut-off voltage	36 V
Fully charge voltage	55.8714 V
Nominal discharge discharge current	52.1739 A
Internal resistance	0.004 Ω

After simulating the model, the output signals are illustrated below:

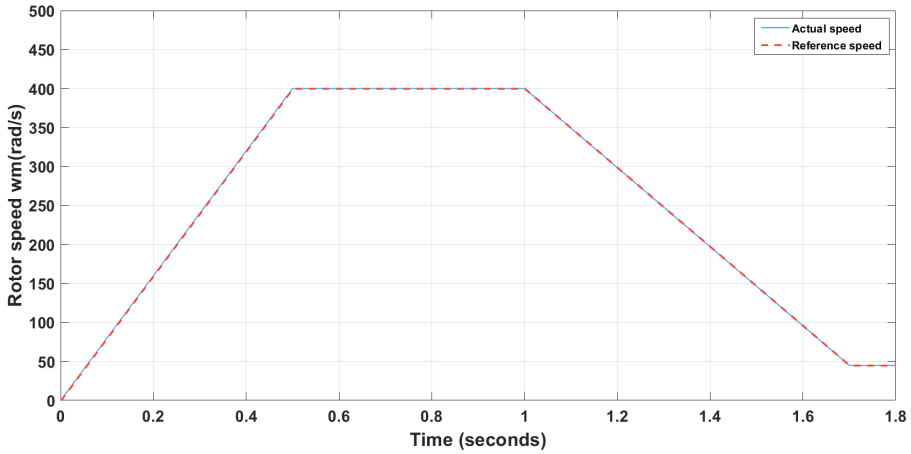

Figure 4.21: Speed response

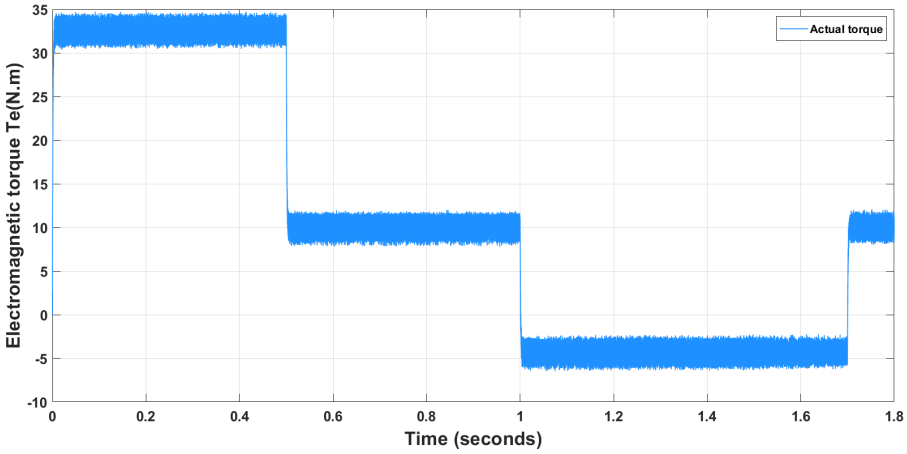

Figure 4.22: Torque resposne

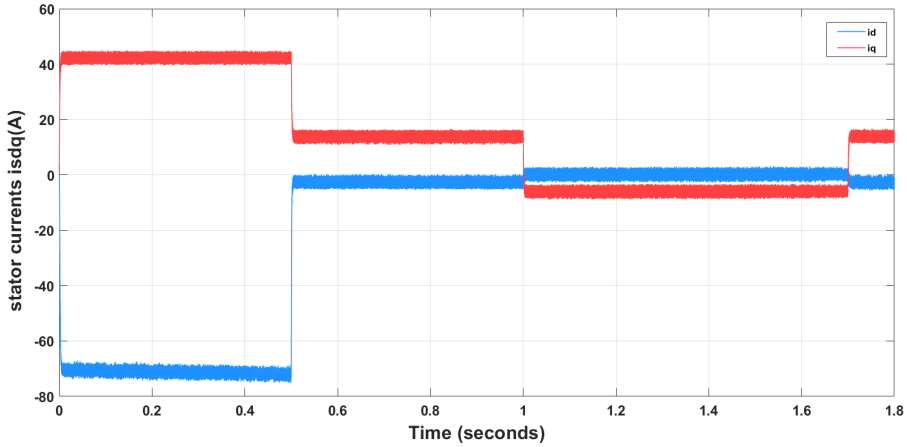

Figure 4.23: dq-axis components of stator currents

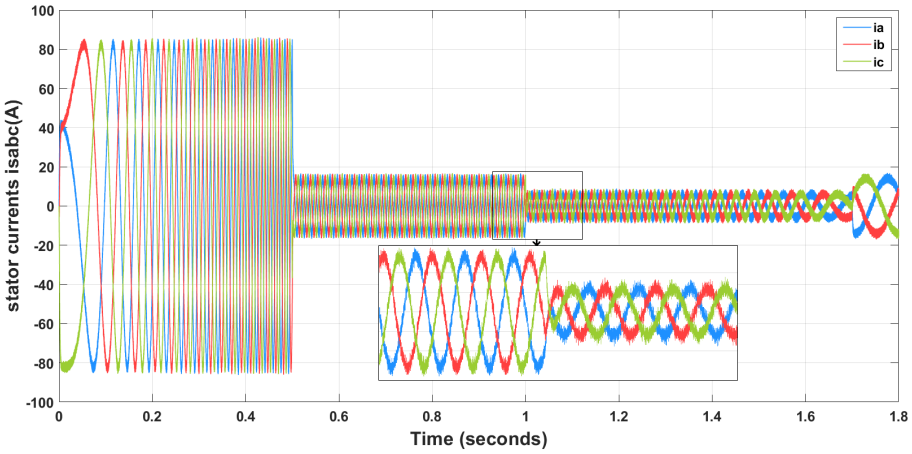

Figure 4.24: Stator currents

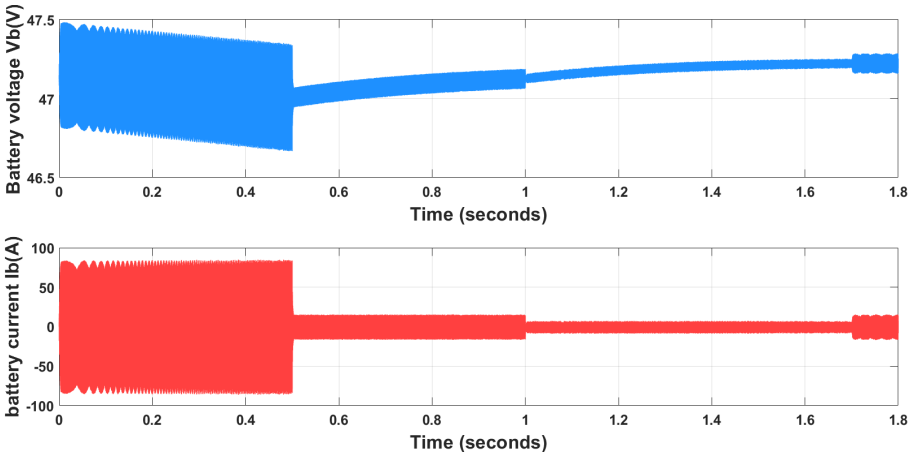

Figure 4.25: Battery outputs

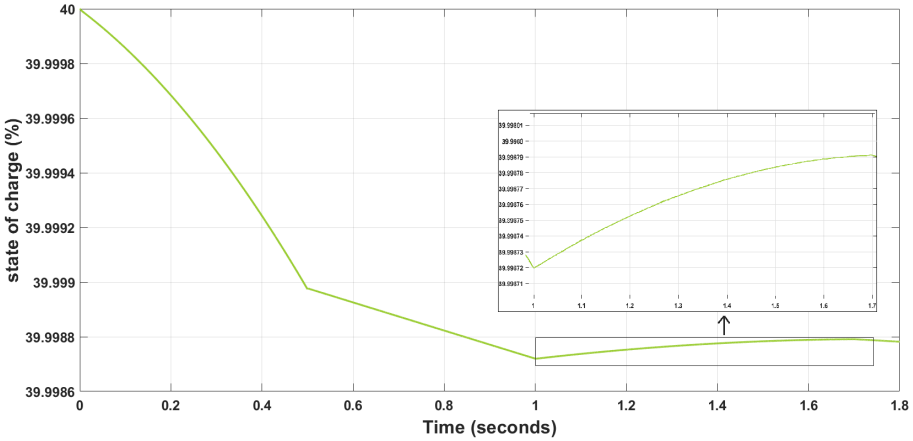

Figure 4.26: Battery voltage and current

Figures 4.21, 4.22, 4.23, and 4.24 display smooth signals. This indicates that powering the motor with a battery pack yields a good performance. Figure 4.25 and 4.26 illustrates the characteristics of one battery. The motor is in driving mode from [0s to 1s], when the motor's speed is increasing and then stays constant ($\frac{dw_e}{dt} \geq 0$). During driving mode, the motor requires a higher DC voltage, hence drawing more voltage from the battery and reducing its state of charge.

The motor is in regenerative mode after 1s, when the motor's speed is decreasing ($\frac{dw_e}{dt} < 0$). During regenerative mode, the motor's kinetic energy is converted into electrical energy which is fed back to the battery, thus recharging the battery and increasing its voltage and state of charge owing to the bidirectional nature of the SVPWM.

4.7.2 With DC-DC converter

Figure 4.27 shows the simulation model for the control of IPMSM using the deadbeat and MTPA controls, supplied by a 6×48V battery pack connected to a half bridge converter.

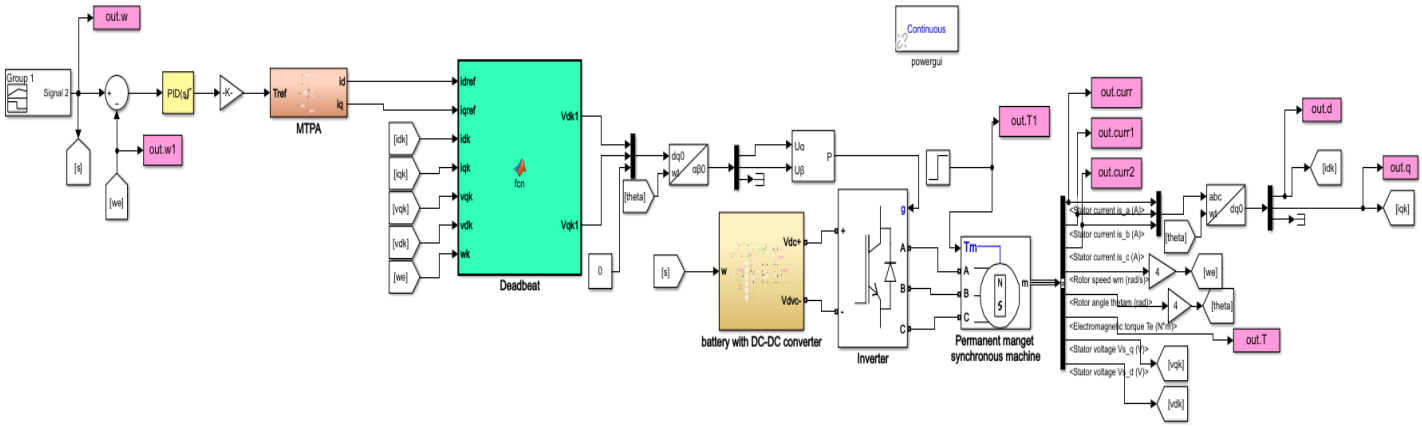

Figure 4.27: Deadbeat control with MTPA controlling IPMSM and DC-DC converter

The parameters for the half bridge converter are shown in table 4.6.

Table 4.6: Converter parameters

Parameter	Value
Capacitor C1	250 μF
Capacitor C2	1000 μF
Resistance R1	0.001 Ω
Resistance R2	10 Ω
Inductance L	10 mH

Figure 4.28 shows the simulation model of the half bridge dc-dc converter with its control system.

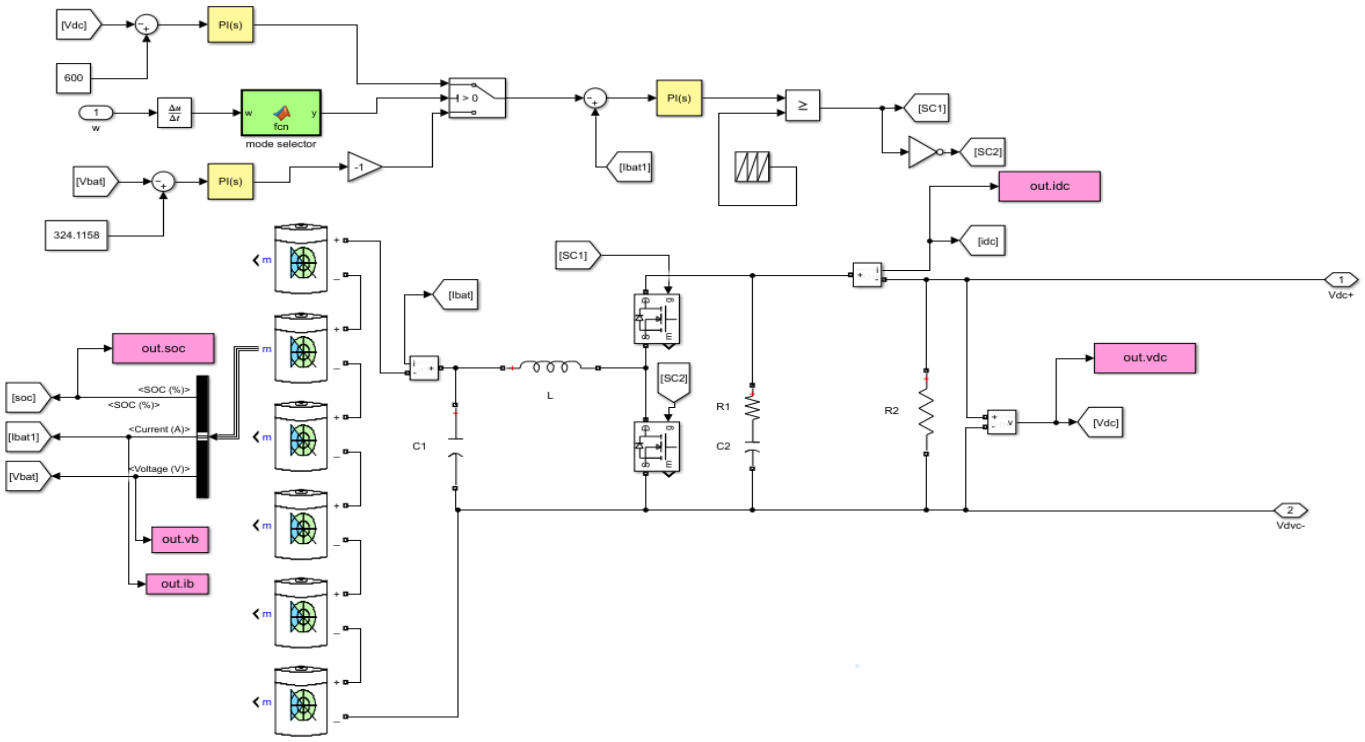

Figure 4.28: Half bridge converter with control system

After simulating the model, the output signals are illustrated below:

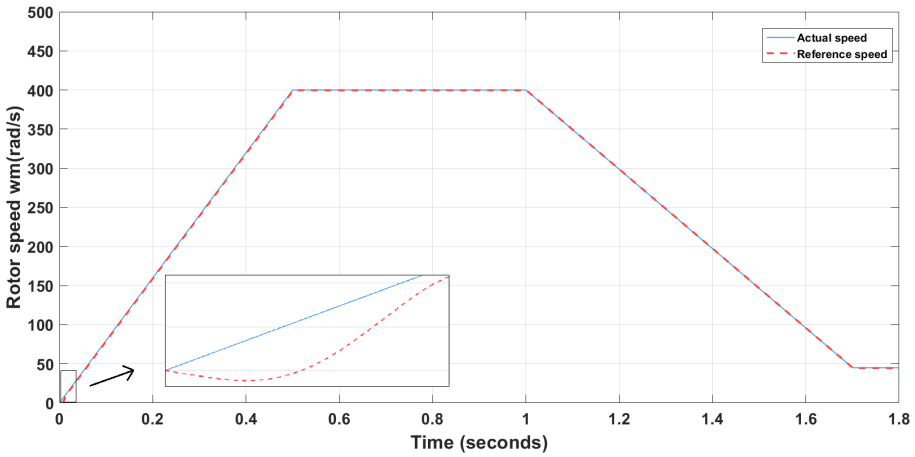

Figure 4.29: Speed response

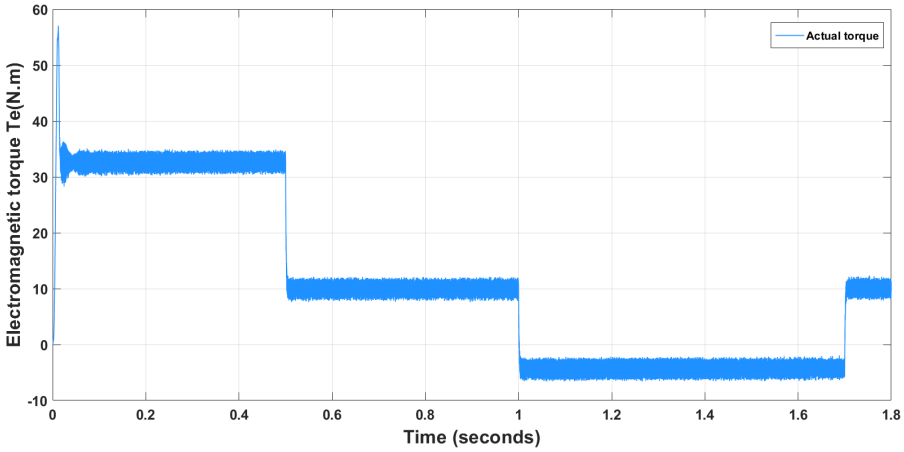

Figure 4.30: Torque response

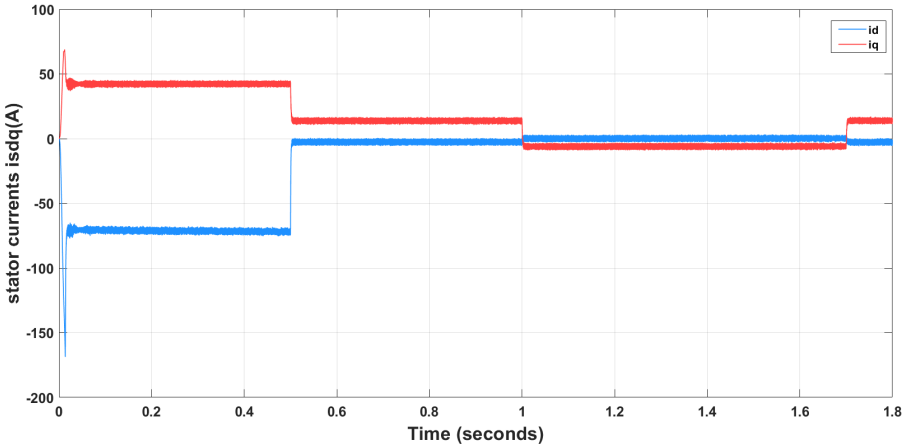

Figure 4.31: dq-axis components of stator currents

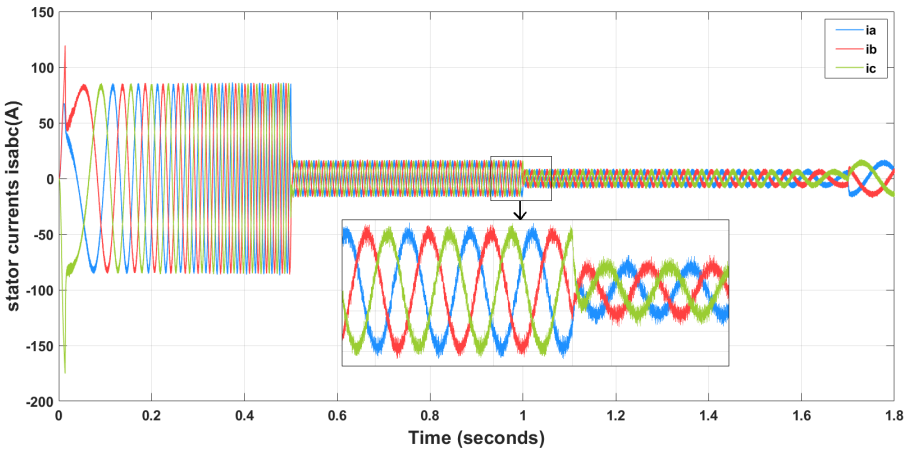

Figure 4.32: Stator currents

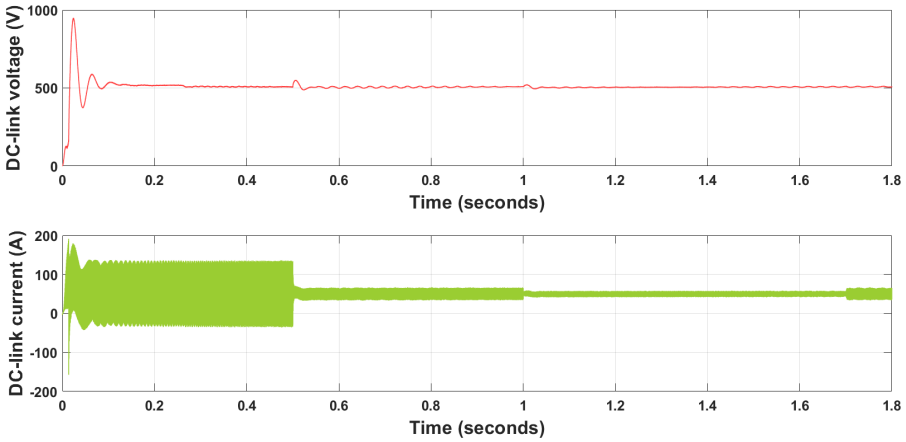

Figure 4.33: DC-link outputs

In figure 4.29, the speed does not reach stability until time 0.01s. This slight delay is a result of the DC-DC converter response time.

The DC-DC converter offered a stable output voltage after 0.1s. It boosted the inverter's input voltage from the battery's voltage level to 600V.

4.8 Conclusion

In this chapter, we explored the different control strategies for IPMSM through simulations. This includes MTPA technique used in field oriented control, deadbeat control, and finite control set model predictive control. Each method demonstrated distinct strengths and weaknesses in terms of response time, accuracy, robustness, and computational complexity.

In field oriented control, the motor's speed follows the reference speed in an excellent manner. However, some harmonics and overshoots can be observed in the currents and torque at the instant at which the speed changes.

Deadbeat control generates a faster response due to the reduced number of PI controllers and results in a smoother and more stable output.

The FCS-MPC generates satisfactory and fast outputs but with some ripples.

The integration of a bidirectional DC-DC converter provided a relatively stable DC voltage to the IPMSM, and reduced the number of batteries needed. The

bidirectional nature of this converter contributed in energy recovery which enhances the efficiency of the system.

Conclusions

This report aims to find the most advantageous control system that optimizes the operation of interior permanent magnet synchronous motor, and therefore enhances the overall performance of the electric vehicle (EV). This is achieved by applying maximum torque per ampere with multiple control techniques: field oriented control (FOC), deadbeat control, finite control set model predictive control (FCS-MPC). These control methods are evaluated by considering various factors such as efficiency, performance, complexity and system constraints.
Maximum Torque per Ampere (MTPA) method excelled in optimizing efficiency, particularly under varying loads, highlighting its advantage in optimizing energy usage and efficiency. Field oriented control gave decent outcomes, however the presence of overshoot could potentially lead to reduced efficiency, increased motor heating and system instability. Finite control set model predictive control (FCS-MPC) and deadbeat control both offered the desired results; fast response, high precision and small ripples, with small differences between them.

In order to power an electric vehicle (EV), the combination of series/parallel connected battery cells is not sufficient. The bidirectional DC-DC converter is an efficient solution to boost the voltage supplied during motoring mode, and recover energy to charge the batteries during regenerative mode, hence extending the lifespan of the batteries.By adjusting the voltage levels, this converter ensures optimal operation of the IPMSM across a wide range of operating conditions, thus

maximizing system efficiency and performance. Furthermore, providing a relatively constant DC-link voltage to the motor contributes in the stability of operation of the motor.

4.9 Future Work

To build on the findings of this research and address the identified limitations, several key areas for future improvement can be considered:

- Simulate the system with variable motor parameters.
- Further improve the control and structure of DC-DC converter for a more stable DC-link voltage.
- Implement experimentally the vehicle traction chain.

Appendix A

Matlab Code for FCS-MPC

```
function [sa,sb,sc] = fcn(e,idr,iqr,id,iq,w,vd1,vq1,Tl,Vdc)
Ld=2.03e-3;
Lq=2.15e-3;
Rs=0.25;
phi=0.12;
J=0.113;
B=0.456e-3;
A=[0 0 0;1 0 0;1 1 0;0 1 0;0 1 1;0 0 1; 1 0 1;1 1 1];
[r,~]=size(A);
T=zeros(r,1);
f=[cos(e);cos(e-2*pi/3);cos(e+2*pi/3)];
n=[-sin(e);-sin(e-2*pi/3);-sin(e+2*pi/3)];
Ts = 1/5000;
for i = 1:8
    iq1=iq*(1 - Ts*Rs/Lq) + Ts/Lq*vq1-w*(Ts*Ld/Lq*id + Ts*phi/Lq);
    id1=id*(1 - Ts*Rs/Ld) + Ts/Ld*vd1+w*(Ts*Lq/Ld*iq);
    vd2=2/3*Vdc*(sum(A(i,:) .* f'));
    vq2=2/3*Vdc*(sum(A(i,:) .* n'));
    w1=w+Ts*1.5*phi*16/(4*J)*iq-Ts*B/J*w-Ts*2/J*Tl+Ts*(1.5*16/(4*J))*(Ld-Lq)
    iqj=iq1*(1 - Ts*Rs/Lq) + Ts/Lq*vq2-w1*(Ts*Ld/Lq*id1 + Ts*phi/Lq);
    idj=id1*(1 - Ts*Rs/Ld) + Ts/Ld*vd2+w1*(Ts*Lq/Ld*iq1);
    T(i,1)=(idr-idj).^2+(iqr-iqj).^2;
end
minval = T(1,1);
mini=1;
for i=2:8
    if T(i,1)<minval
        minval=T(i,1);
        mini=i;
    end
end
sal=A(mini,1);
sbl=A(mini,2);
scl=A(mini,3);
sa=boolean(sal);
sb=boolean(sbl);
sc=boolean(scl);
```

Figure A.1

Bibliography

[1] Xiaoli Sun, Zhengguo Li, Xiaolin Wang, and Chengjiang Li. Technology development of electric vehicles: A review. *Energies*, 13(1):90, 2019.

[2] Xin Yuan, Shuo Zhang, and Chengning Zhang. Enhanced robust deadbeat predictive current control for pmsm drives. *IEEE Access*, 7:148218–148230, 2019.

[3] Jose Rodriguez and Patricio Cortes. *Predictive control of power converters and electrical drives*. John Wiley & Sons, 2012.

[4] Leon Christopher Rosario. *Power and energy management of multiple energy storage systems in electric vehicles*. PhD thesis, 2007.

[5] M. Spendiff-Smith. Electric vehicles types - a complete guide to types of ev - evesco, March 18 2022. https://www.power-sonic.com/blog/types-of-electric-vehicles.

[6] Vijay Tharad. Overview of ev battery technology through battery characteristics and parameters, October 18 2023. https://www.linkedin.com/pulse/overview-ev-battery-technology-through-parameters-vijay-tharad-0t42c.

[7] Ruoyu Xu. Lithium-ion battery modeling and soc estimation, 2023.

[8] C. Jaszczolt. Understanding permanent magnet motors, January

31 2017. https://www.linkedin.com/pulse/overview-ev-battery-technology-through-parameters-vijay-tharad-0t42c.

[9] Omer Can Tolun and Onder Tutsoy. 3d modeling and justification of an electrical vehicle with multibody modeling softwares. In *5th International Conference on Life and Engineering Sciences*, 2022.

[10] C Nevoloso et al. *Enhanced mathematical modelling of interior permanent magnet synchronous machines for loss minimization control*. PhD thesis, 2020.

[11] Kharagpur. Introduction to voltage source inverters, n.d.

[12] geeksforgeeks. 3-phase inverter, February 27 2024. https://www.linkedin.com/pulse/overview-ev-battery-technology-through-parameters-vijay-tharad-0t42c.

[13] Ramu Krishnan. *Electric motor drives: modeling, analysis, and control*. Prentice Hall, 2001.

[14] D. Collins. What is space vector pulse width modulation (svpwm)?, n.d. https://www.motioncontroltips.com/what-is-space-vector-pulse-width-modulation-svpwm/.

[15] Gussay Abdalrahman, Othman Hassan Abdalla, Mohamed Ismail Jibril, and Ahmed A Awad. Space vector pulse width modulation technique applied to two level voltage source inverter. 2018.

[16] D. Anandarup. Space vector pwm, n.d.

[17] J. Wimmer. Lithium-ion battery modeling for the automotive engineer, December 8 2021. https://www.gtisoft.com/blog-post/lithium-ion-battery-modeling-for-the-automotive-engineer/.

[18] Zhai Haizhou. Modeling of lithium-ion battery for charging/discharging characteristics based on circuit model. *International Journal of Online Engineering*, 13(6), 2017.

[19] Werner Leonhard. *Control of electrical drives*. Springer Science & Business Media, 2001.

[20] Weiwei Zhang, Fei Xiao, Jilong Liu, Zhiqin Mai, and Chaoran Li. Maximum torque per ampere control for ipmsm traction system based on current angle signal injection method. *Journal of Electrical Engineering & Technology*, 15:1681–1691, 2020.

[21] Osman Emre Özçiflikçi, Mikail Koç, and Serkan Bahçeci. Maximum torque per ampere strategy in ipm drives for electric vehicles. *El-Cezeri*, 8(3):1405–1415, 2021.

[22] Gómez Corlos. Predictive control for pmsm. *Master's Thesis, Department of Energy Technology, Aalborg University, Denmark*, 2016.

[23] Jesper Moos. Predictive deadbeat control for pmsm drive. *Master's Thesis, Department of Energy Technology, Aalborg University, Denmark*, 2014.

[24] Francis Mwasilu, Hoach The Nguyen, Han Ho Choi, and Jin-Woo Jung. Finite set model predictive control of interior pm synchronous motor drives with an external disturbance rejection technique. *IEEE/ASME Transactions on Mechatronics*, 22(2):762–773, 2016.

[25] Francis Mwasilu, Eun-Kyung Kim, Muhammad Saad Rafaq, and Jin-Woo Jung. Finite-set model predictive control scheme with an optimal switching voltage vector technique for high-performance ipmsm drive applications. *IEEE Transactions on Industrial Informatics*, 14(9):3840–3848, 2017.

[26] Mustafa Inci and Ömer Türksoy. Review of fuel cells to grid interface: Configurations, technical challenges and trends. *journal of cleaner Production*, 213:1353–1370, 2019.

[27] Shivani Dhanaji Mane Poonam Ramesh Mane Ruchita Sanjay Patil Pranali Suresh Bhosale M.S.Kulkarni, Namrata Nishikant Patil. Design and implementation of non-isolated half bridge dc-dc bidirectional converter using fuzzy logic. *MAT Journals*, 4(2), 2019.

[28] Toshi Sharma and Avik Bhattacharya. Performance analysis of encoderless dtc of ipmsm for wide operating range. *Arabian Journal for Science and Engineering*, 45:6501–6515, 2020.